Results

Longitudinal growth retardation in KMI (mri/mri)

KMIs developed dwarfism with short limbs and trunk compared to the wild-type littermates (Fig. 1A). Growth curves indicated that KMIs started to show the axial growth retardation postnatally at 4 wk of age, although there was no difference between wild-type and heterozygote (+/*mri*) rats in either sex, confirming an autosomal recessive inheritance (Fig. 1B). The trunk of the KMIs was about 30% shorter than those of wild-type and +/*mri* littermates at 10 wk of age. Skeletal X-ray analysis at this age revealed no appreciable changes between wild type and KMI in the width of calvarium, which is formed through intramembranous ossification; however, the longitudinal lengths of femora, tibiae, and vertebrae, all of which are formed through endochondral ossification, were 20%–30% shorter in KMI than in wild type (Fig. 1C,D). In the long bones of KMI, the height of the epiphyseal growth plate was greater than that in wild type, indicating that the growth retardation in KMI resulted from the impairment of endochondral ossification in the growth plate.

Positional cloning of the mri *mutation*

We first genotyped simple sequence length polymorphism (SSLP) markers throughout the rat genome on the backcross progeny and detected putative linkage at the *D14Rat6* marker on rat chromosone 14. Further genetic mapping localized the *mri* locus to a 1.2-cM interval on rat chromosome 14 flanked by markers *D14Rat5* and *D14Rat80*. Comparative mapping analysis revealed that the region was orthologous to the regions on mouse chromosome 5 and human chromosome 4, in which several candidate genes including *Bmp3* and *cGKII* (also known as *Prkg2*) were identified (Fig. 2A). Although the *Bmp3* gene encoding a bone morphogenetic protein (BMP) first drew our attention, our studies revealed this gene unlikely to be causative of the KMI phenotype. The expression of the *Bmp3* gene was not different between wild type and KMI, and the sequencing analysis showed only a few silent variants (data not shown). Furthermore, the *Bmp3* null mice are reported to exhibit normal body size but increased bone density (Daluiski et al. 2001), which is different from the KMI phenotypes.

We then performed an RT–PCR analysis of the *cGKII* gene, and found that the cGKII transcript from the brain of the KMI mutant was shorter than that from wild type (Fig. 2B). Sequencing analysis disclosed that exon 3 of the *cGKII* gene was directly spliced onto exon 6 (Fig. 2C). This 220-bp deletion spanning exons 4 and 5 resulted in a frame shift and a premature stop codon, predicting a truncated product that lacks the entire kinase domain (Fig. 2D). We further carried out inter-exon PCR between exons 3 and 6 of the genomic DNA, and found an ~5-kb

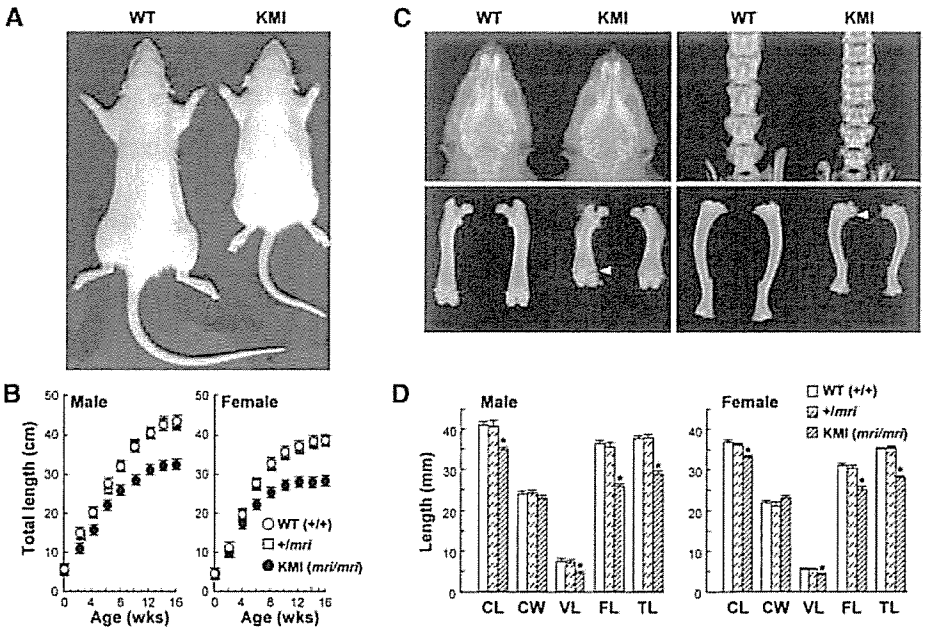

Figure 1. Longitudinal growth retardation in KMI (*mri/mri*). (*A*) Gross appearance of wild-type (WT) and KMI littermates at 10 wk of age. (*B*) Growth curves of wild-type (WT; +/+), heterozygote (+/*mri*), and homozygote (KMI, *mri/mri*) rats determined by the total axial length (from nose to tail end). The symbols of +/*mri* are behind those of wild-type rats. Data are expressed as means (symbols) ± S.E.M. (error bars) for 12 rats/group. (*C*) Plain X-ray images of heads (*top left*), lumbar vertebrae (*top right*), femora (*bottom left*), and tibiae (*bottom right*) of wild-type (WT) and KMI littermates at 10 wk. Arrowheads indicate the expanded growth plates in KMI. (*D*) Bone lengths of wild type (WT), +/*mri*, and KMI at 10 wk. (CL) Naso-occipital length of the calvarium; (CW) maximal interparietal distance of the calvarium; (VL) fifth lumbar vertebral length; (FL) femoral length; (TL) tibial length. Data are means (bars) ± S.E.M. (error bars) for 12 rats/group. (*) $P < 0.05$ vs. wild type.

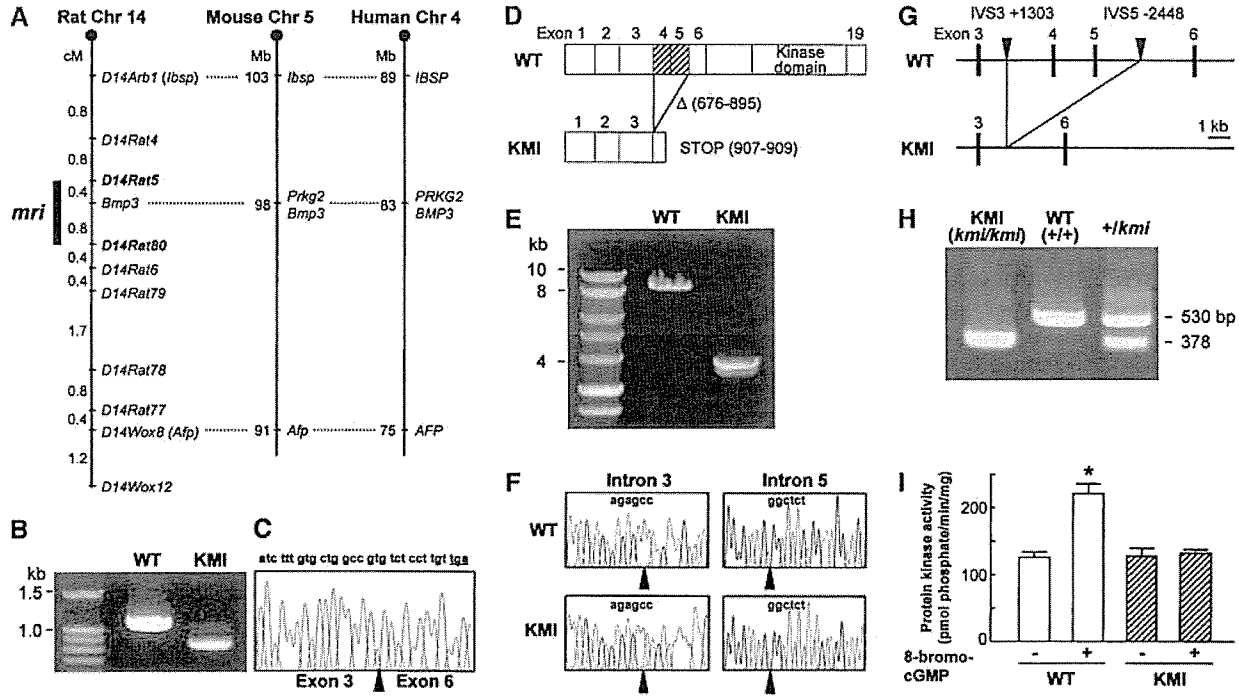

Figure 2. Identification of the *mri* mutation. (*A*) Comparative mapping of the *mri* region in the rat, mouse, and human choromosomes. The *mri* locus, which was mapped to a 1.2-cM interval between markers *D14rat5* and *D14rat80*, is shown as a bold line. (*B*) RT–PCR products of the rat cGKII from the brains of wild-type (WT) and KMI littermates. (*C*) Sequence analysis of transcript of the *cGKII* gene from the KMI mutant. Exon 3 is directly spliced onto exon 6, with the boundary indicated by the arrowhead. The frame shift causes amino acid substitutions and a premature stop codon. (*D*) Schematic representation of the prematurely truncated cGKII protein in the KMI mutant. Nucleotide sequence analyses of the cDNA identified a 220-bp deletion (676–895) corresponding to exons 4 and 5. (*E*) Interexon PCR between exons 3 and 6 using the genomic DNA from wild type (WT) and KMI indicated an ~5-kb deletion in the KMI. (*F*) Sequence analyses of genomic DNA of wild type (WT) and KMI identified breakpoints in introns 3 and 5 (arrowheads). A common sequence, "AGAGCC", was found at the two breakpoints. (*G*) Schematic representation of the *mri* mutation as an ~5-kb deletion in the *cGKII* gene. Sequence analyses disclosed the deletion from IVS3+1303 to IVS5–2448 in KMI. (*H*) Genotyping of KMI (*mri/mri*), wild-type (WT; +/+), and +/*mri* rats. A longer amplicon (530 bp) was amplified from wild-type allele, and a shorter amplicon (378 bp) from the mutated allele. (*I*) Lack of cGMP-dependent protein kinase activity of the KMI brain extract determined by the in vitro kinase assay in the presence and absence of 8-bromo-cGMP. Data are means (bars) ± S.E.M. (error bars) of six samples/group. (*) $P < 0.01$, significant effect of 8-bromo-cGMP.

deletion in the *cGKII* gene of KMI (Fig. 2E). Sequencing analysis identified the breakpoints in introns 3 and 5, both of which had a common sequence, "AGAGCC" (Fig. 2F), creating a deletion from intervening sequence (IVS)3+1303 to IVS5–2448 (Fig. 2G). To confirm that this deletion in the *cGKII* gene was responsible for the KMI phenotype, we designed PCR primers to detect this genomic deletion, and found complete cosegregation of the genotypes KMI (*mri/mri*), wild type (+/+), and +/*mri* with the phenotypes (Fig. 2H). To test whether the *mri* mutation in the *cGKII* gene resulted in loss of its function, tissue extract from brain that is known to express high levels of cGKII was assayed for the kinase activity. The in vitro kinase assay revealed that the wild-type extract showed a significant increase in the kinase activity by the stimulation with the cGMP analog 8-bromo-cGMP; however, the increase was not observed in the KMI extract (Fig. 2I). Taken together, these results strongly suggested that the deletion in the *cGKII* gene resulted in loss of its function and caused dwarfism in KMI.

Abnormal endochondral ossification in the growth plate and the fracture callus of KMI

We first investigated the expression pattern of cGKII in the proximal growth plates of the wild-type and KMI tibiae at 10 wk of age. Immunohistochemical analysis of the wild-type growth plate revealed that cGKII was expressed predominantly in the late proliferative and prehypertrophic chondrocytes, preceding the start of hypertrophic differentiation; however, no immunoreactivity for cGKII was observed in the KMI growth plate (Fig. 3A, α-cGKII).

To elucidate the cellular mechanisms underlying the dwarfism due to the cGKII dysfunction in KMI, we performed histological analyses of the growth plates. At birth, growth plates showed no discernible difference between wild type and KMI (Fig. 3A, HE, E18.5). Pathological changes gradually became evident postnatally after 4–5 wk of age, and at 10 wk the height of the KMI growth plate was about 2.5-fold greater than that of wild type

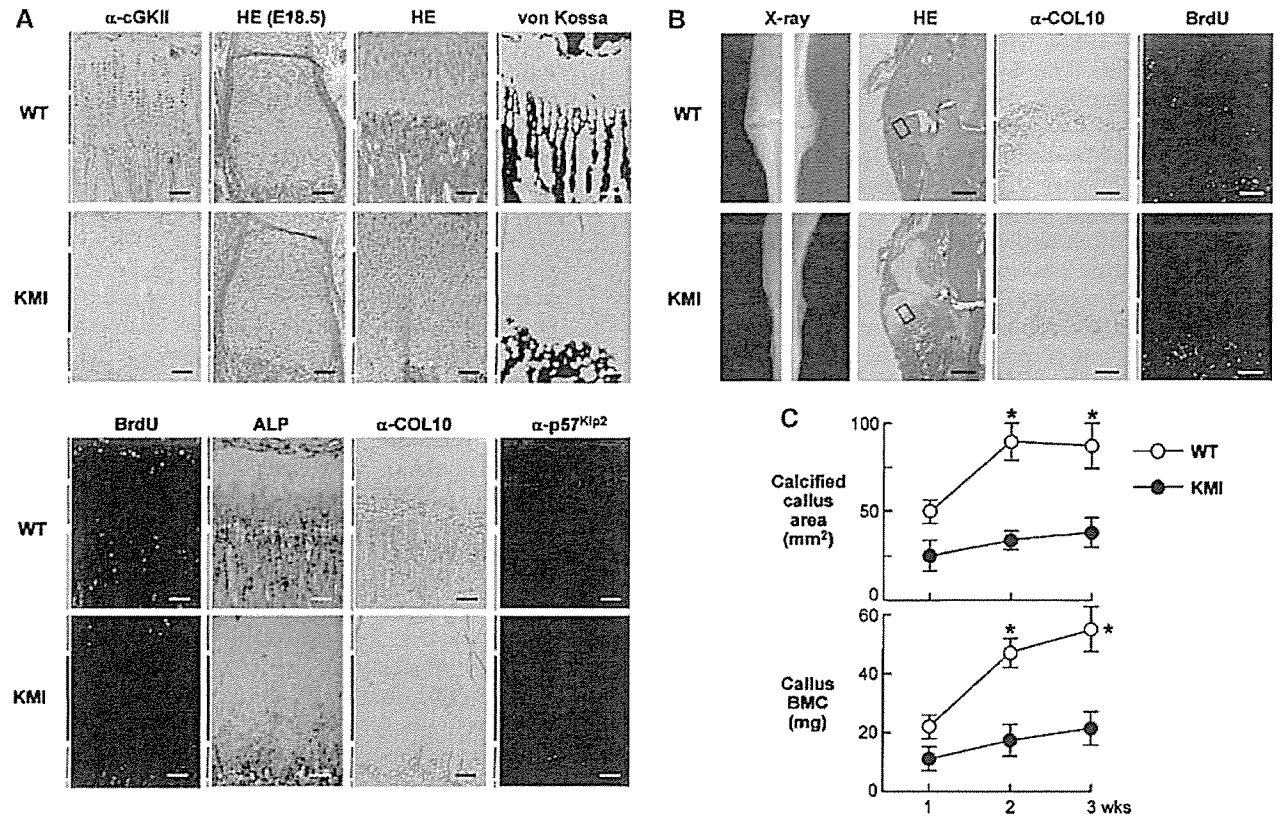

Figure 3. Comparison of endochondral ossification in the growth plate (*A*) and the bone fracture callus (*B*,*C*) between wild type (WT) and KMI. Blue, red, and green bars indicate layers of proliferative zone, hypertrophic (including prehypertrophic) zone, and primary spongiosa, respectively. Black bar indictates the abnormal intermediate zone that is seen only in KMI. (*A*) Histological findings of the proximal growth plates in wild-type (WT) and KMI tibiae at 10 wk of age unless otherwise described. (*Upper* panel) Immunohistochemical staining with an anti-cGKII antibody (α-cGKII), hematoxylin-eosin staining of the humeral growth plates of fetal rats (HE, E18.5), HE staining (HE), and von Kossa staining (von Kossa). (*Lower* panel) BrdU labeling (BrdU), alkaline phosphatase staining (ALP), immunohistochemical stainings with anti-type X collagen (α-COL10), and anti-p57^{Kip2} (α-p57^{Kip2}) antibodies. Bars, 50 μm. (*B*) Radiological and histological findings of the fracture callus 2 wk after the surgery. After exposing the right tibiae of 10-week-old rats, a transverse osteotomy was performed at the midshaft with a bone saw and was stabilized with an intramedullary nail. Plain X-ray images (X-ray), HE staining (HE; *inset* boxes indicate the regions of the *right* two figures), immunohistochemical staining with an anti-type X collagen antibody (α-COL10), and BrdU labeling (BrdU). Bars: HE, 500 μm; *right* two figures, 50 μm. (*C*) Time course of the calcified area and the bone mineral content (BMC) of the callus at the fracture site measured by a single energy X-ray absorptiometry. Data are mean (symbols) ± S.E.M. (error bars) of eight rats/genotype. (*) $P < 0.01$ vs. wild type.

(665 ± 47 μm vs. 255 ± 34 μm, mean ± S.E.M., $n = 8$, respectively), although the columnar structure was relatively preserved (Fig. 3A, HE). This increase was due to an intermediate layer of accumulated abnormal chondrocytes in the KMI growth plate (Fig. 3A, HE, black bar). Although the cell size of chondrocytes in the KMI hypertrophic zone seemed somewhat smaller than that in wild type, matrix mineralization determined by von Kossa staining appeared normal in KMI (Fig. 3A, von Kossa).

To further characterize the abnormal chondrocytes in the intermediate layer of the KMI growth plate, we examined cellular proliferation by the the uptake of BrdU. In wild type, chondrocytes in the proliferating zone and bone marrow cells in the primary spongiosa were actively proliferating as detected by the BrdU uptake (Fig. 3A, BrdU). In KMI, the number of BrdU-positive cells was slightly decreased in the proliferating zone, and more importantly, no uptake was observed in the intermediate layer, suggesting that these abnormal chondrocytes were postmitotic. We next examined the distributions of alkaline phosphatase (ALP) and type X collagen (COL10) as markers of prehypertrophic and hypertrophic chondrocytes, respectively. Histochemical analyses of the wild-type growth plate revealed that these markers were expressed immediately after the BrdU uptake had disappeared, confirming the coupling of the cessation of proliferation and the start of hypertrophic differentiation (Fig. 3A, ALP and α-COL10). In the KMI growth plate, however, the intermediate layer was stained by neither of the markers, indicating that these abnormal chondrocytes had not started hypertrophic differentiation. In addition, expression of p57^{Kip2}, a key regulator of cell-cycle arrest and differentiation of chondrocytes (Yan et al.

1997; Stewart et al. 2004) was limited to the boundary of proliferative and hypertrophic zones in the wild-type growth plate (Fig. 3A, α-$p57^{Kip2}$), whereas in KMI the $p57^{Kip2}$-expressing cells were broadly and sporadically scattered in the intermediate layer, suggesting a loss of synchronized withdrawal from the cell cycle of the chondrocytes. Hence, the intermediate layer chondrocytes were abnormal cells that had ceased proliferation but had not started hypertrophic differentiation.

To examine whether cGKII has an important role generally for endochondral ossification, we compared the healing process of bone fracture produced by a transverse osteotomy and stabilized with an intramedullary nail at the midshaft of tibiae of wild type and KMI (Shimoaka et al. 2004). X-ray analysis 2 wk after the fracture showed substantial calcified callus formation in wild type, which was rarely seen in KMI (Fig. 3B, X-ray). Time course analyses of the calcified area and the bone mineral content (BMC) of the callus measured by a bone densitometer revealed the impairment of endochondral ossification in KMI at 2 wk and thereafter (Fig. 3C). Histological analysis at 2 wk confirmed that endochondral ossification was present in the wild-type fracture callus; in KMI, however, massive uncalcified cartilagenous callus remained, although intramembranous ossification from the periosteum was normally seen (Fig. 3B, HE). When distributions of hypertrophic and proliferating chondrocytes were examined by the COL10 immunostaining and the BrdU uptake, respectively, the two kinds of cells were located adjacent to each other in the wild-type callus, indicating the tight coupling between proliferation and hypertrophic differentiation in this model as well (Fig. 3B, α-COL10 and BrdU). In the KMI callus, there was an intermediate layer with an accumulation of abnormal cells that were stained by neither marker (Fig. 3B, black bars), as observed in the growth plate.

Taking these histological findings together, the cessation of proliferation and the start of hypertrophic differentiation, which were tightly coupled under normal conditions, were dissociated in both the growth plate and the fracture callus of KMI. The cGKII dysfunction was therefore shown to impair the synchronized switching from proliferation to hypertrophic differentiation of chondrocytes in the endochondral ossification.

Functions of cultured chondrocytes from KMI growth plate

To investigate the mechanism underlying the abnormality of chondrocytes due to the cGKII deficiency, ex vivo cultures of primary chondrocytes isolated from the proximal growth plates of the wild-type and KMI tibiae were performed. We first compared the time course of cell proliferation determined by the growth curve for 8 d, and found no significant difference between wild-type and KMI chondrocytes (Fig. 4A). However, after 5 d of culture when the chondrocytes became confluent, the cell shape by the phase contrast image was different between wild type and KMI: The former was hexagonal whereas the latter showed a spindle-shape appearance (Fig. 4B). ALP staining revealed that the KMI chondrocytes were less differentiated than wild type. In addition, a real-time RT–PCR analysis revealed that the expression of COL10, a marker for hypertrophic differentiation, was down-regulated in cultured KMI chondrocytes compared to wild-type chondrocytes. To confirm the contribution of cGKII to these abnormalities, cGKII was introduced into cultured KMI chondrocytes using an adenovirus vector carrying the *cGKII* gene (Ax-*cGKII*). As a result, the suppression of all of these differentiation markers in the KMI culture was restored to those similar to the wild-type culture, although introduction of the same adenovirus vector without the *cGKII* gene (Ax-vector) did not affect them (Fig. 4B).

We next examined the involvement of cGKII in the putative signalings which regulate hypertrophic differentiation of chondrocytes (Fig. 4C,D). PTH/PTHrP via the cAMP-dependent protein kinase (PKA) is known to be a major signal in the inhibition of chondrocyte hypertrophy (Chung and Kronenberg 2000). PTHrP and PTH/PTHrP receptor levels were similar between the wild-type and KMI cultures, and PTH/PTHrP signaling determined by the dose-response effect of PTH on cAMP accumulation was not enhanced in the KMI chondrocyte culture compared to the wild-type culture, indicating that the impaired differentiation of the KMI chondrocytes is not due to a defect of the inhibition by cGKII on the PTH/PTHrP signaling (Fig. 4C). C-type natriuretic peptide (CNP) is also known to be a positive regulator of endochondral ossification and a putative ligand for cGKII (Chusho et al. 2001; Miyazawa et al. 2002). Addition of CNP failed to rescue either the impaired ALP activity or the COL10 expression in the KMI chondrocyte culture (Fig. 4D), indicating that cGKII plays a role in CNP-mediated chondrocyte differentiation. On the other hand, BMP-2 potently increased these differentiation markers, suggesting that the BMP signaling molecules Smads and Runx2 may be independent of the cGKII signaling (Fig. 4D). These results demonstrate that cGKII is not involved in the two major signalings of chondrocyte hypertrophy: PTH/PTHrP and BMP.

cGKII as an attenuator of Sox9 function

We further examined the involvement of cGKII in the function of Sox9, a transcription factor that is known to be essential for chondrogenic differentiation of mesenchymal cells (de Crombrugghe et al. 2001). Sox9 also functions as a potent inhibitor of the hypertrophic differentiation of chondrocytes (Akiyama et al. 2002), and the expression disappears at the hypertrophic zone in the growth plate (Huang et al. 2000). In line with previous studies, our immunohistochemical study confirmed the lack of Sox9 localization in the hypertrophic zone of the wild-type growth plate; however, nuclear localization of Sox9 was clearly visible in the abnormal intermediate layer of the KMI growth plate (Fig. 5A).

To assess the possible interaction between cGKII and Sox9, we performed transfection experiments with plasmids encoding cGKII and/or Sox9 in cell culture sys-

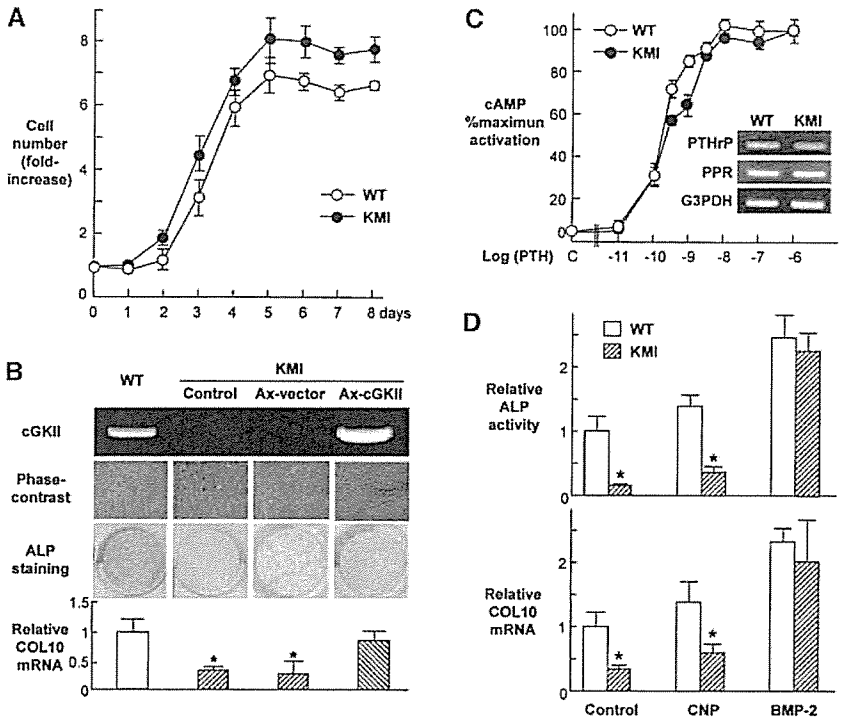

Figure 4. Functions of cultured chondrocytes from wild type and KMI. (*A*) Growth curves of wild-type (WT) and KMI chondrocytes isolated from the growth plate. Data are mean (symbols) ± S.E.M. (error bars) of six dishes/genotype. Lack of significant difference between the genotypes was confirmed in five independent experiments. (*B*) Differentiation of wild-type (WT) and KMI chondrocytes determined by the phase contrast image, ALP staining, and COL10 mRNA level determined by real-time quantitative RT–PCR cultured for 5, 21, and 28 d, respectively. As a rescue experiment, an adenovirus vector carrying the *cGKII* gene (Ax-*cGKII*) or that without the *cGKII* gene (Ax-vector) was introduced into KMI chondrocytes. (*Top* panel) The cGKII mRNA level is shown by RT–PCR. COL10 mRNA levels are mean (bars) ± S.E.M. (error bars) of the relative amount of mRNA compared to that of wild type of six wells/group. (*) $P < 0.05$ vs. wild type. (*C*) PTH/PTHrP signaling determined by the dose-response effects of PTH (10^{-11} to 10^{-6} M) on cAMP accumulation in wild-type (WT) and KMI chondrocytes. Data are mean (symbols) ± S.E.M. (error bars) of the percentages of maximal cAMP activation for six wells/genotype. Lack of significant difference between the genotypes was confirmed in three independent experiments. The PTHrP and PTH/PTHrP receptor (PPR) mRNA levels are shown by RT–PCR as an *inset*. (*D*) Effects of CNP (100 nM) and BMP-2 (100 ng/mL) on the ALP activity and COL10 mRNA level determined by real-time quantitative RT–PCR in the wild-type (WT) and KMI chondrocyte cultures for 21 and 28 d, respectively. Data are mean (bars) ± S.E.M. (error bars) of six wells/group. (*) $P < 0.01$ vs. wild type.

tems. Initially, to know the effects of cGKII and Sox9 on the hypertrophic differentiation of chondrocytes, we examined the COL10 expression in cultured mouse chondrogenic ATDC5 cells (Fig. 5B; Shukunami et al. 1996). In the monolayer culture, the baseline of the COL10 level was low and little altered by the Sox9 transfection; however, in the three-dimensional culture, ATDC5 cells differentiated into hypertrophic chondrocytes with COL10 expression in the presence of insulin, as reported previously (Seki et al. 2003). The Sox9 transfection was confirmed to reduce the COL10 mRNA level, and the cotransfection with cGKII restored it to the control level. In addition, transfection with Sox9 was also confirmed to show an ~10-fold increase in the type II collagen (COL2) mRNA level in human nonchondrogenic hepatoma HuH-7 cells, and cotransfection with cGKII significantly suppressed the Sox9-induced COL2 expression (Fig. 5C). These results suggest a novel function of cGKII as an attenuator of the Sox9 actions: inhibition of hypertrophic differentiation and stimulation of chondrogenic differentiation. We further examined the effects of mutated cGKII: one derived from KMI (cGKII-KMI) and the other lacking the entire kinase domain (cGKII-Δkinase) in the respective cultures (Fig. 5B,C). Neither of the mutant cGKIIs restored the Sox9-inhibited COL10 level nor suppressed the Sox9-induced COL2, implicating that the kinase activity of cGKII was indispensable for the attenuation of the Sox9 function. Hence, we next examined the involvement of phosphorylation of Sox9 in the action of cGKII. The consensus amino acid sequence for phosphorylation by cGKII is RRXS/TX where either S or T is the phosphorylation site (Hofmann 1995), and a single consensus sequence was detected at Ser 181 (S181) in the human Sox9. Immunoblot analysis with a phosphorylation-specific antibody revealed that the cGKII cotransfection stimulated the phosphorylation of transfected Sox9 at S181 in HuH-7 cells (Fig. 5D, top panel). To learn the functional relevance of the Sox9 phosphorylation by cGKII, we generated a phosphorylation-deficient Sox9 vector ($Sox9^{S181A}$) by introducing serine-to-alanine substitutions at S181. The $Sox9^{S181A}$ transfection induced the COL2 expression to a level similar to that of the wild-type Sox9 in HuH-7 cells (Fig. 5D, bottom panel). Interestingly, the cGKII cotransfection decreased the COL2 induction by the $Sox9^{S181A}$ similarly to that by the wild-type Sox9, indicating that the phosphorylation of Sox9 itself is dispensable for the attenuation of the Sox9 function by cGKII.

To clarify the mechanism underlying the attenuation of the Sox9 signaling by cGKII, we examined the subcellular localization of Sox9. Fluorescent images of HeLa cells transfected with the plasmid encoding GFP-Sox9 revealed that Sox9 is predominantly localized in the nucleus, in agreement with previous reports (Fig. 6A; Huang et al. 2001). When cGKII was cotransfected, Sox9 became localized not only in the nucleus, but also in the

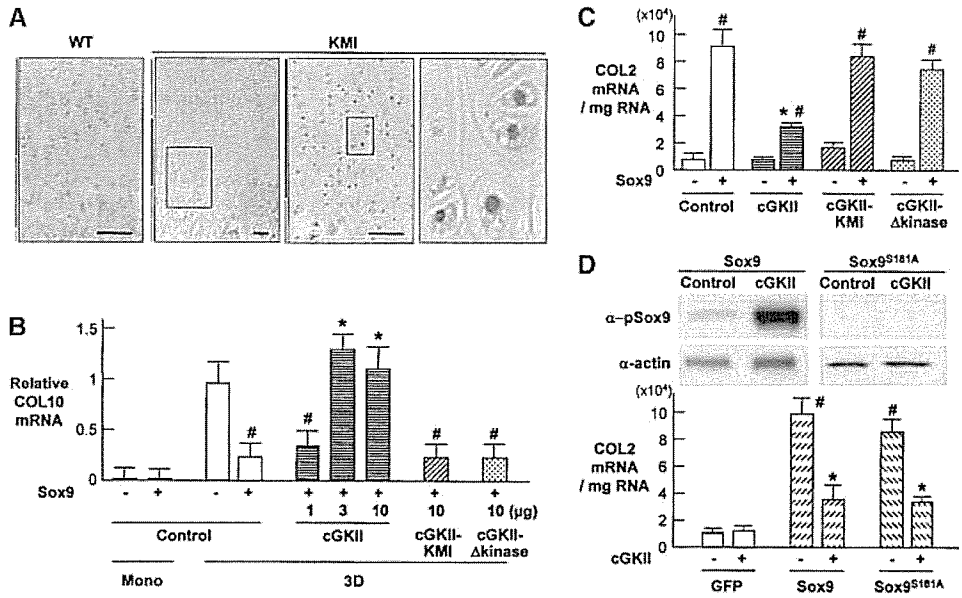

Figure 5. Regulation of Sox9 function and phosphorylation by cGKII. (*A*) Immunohistochemical stainings with an anti-Sox9 antibody in the growth plates of the proximal tibiae of wild type (WT) and KMI at 10 wk of age. *Inset* boxes in the *middle* two panels indicate the regions of the respective *right* panels. Blue, black, red, and green bars indicate layers of proliferative zone, abnormal intermediate zone, hypertrophic zone, and primary spongiosa, respectively. Bar, 50 μm. (*B*) COL10 mRNA levels by the transfection with the plasmid encoding Sox9 determined by real-time quantitative RT–PCR in cultured ATDC5 cells cotransfected with the empty vector (control), the expression vectors of cGKII (1, 3 and 10 μg), cGKII-KMI (10 μg), and cGKII-Δkinase (10 μg) in the monolayer culture (Mono) and three-dimensional alginate beads culture (3D) in the chondrogenic medium with insulin. Data are mean (bars) ± S.E.M. (error bars) of six wells/group. (#) $P < 0.01$, significant inhibition by Sox9. (*) $P < 0.01$, significant stimulation by cGKII. (*C*) Induction of COL2 mRNA by the Sox9 transfection determined by real-time quantitative RT–PCR in cultured HuH-7 cells cotransfected with the empty vector (control), the expression vectors of wild-type cGKII (cGKII), the mutated cGKII lacking exons 4 and 5 (cGKII-KMI), and that lacking the kinase domain (cGKII-Δkinase). Data are mean (bars) ± SEM (error bars) of six wells/group. (#) $P < 0.01$, significant stimulation by Sox9. (*) $P < 0.01$, significant inhibition by cGKII. (*D*, *top*) Immunoblotting with an anti-phosho-Sox9 antibody (α-pSox9) in cultured HuH-7 cells transfected with wild-type Sox9 or phosphorylation-deficient Sox9 ($Sox9^{S181A}$). Blottings with anti-β-actin (α-actin) were used as loading control. (*Bottom*) Induction of COL2 mRNA by the transfection with Sox9 or $Sox9^{S181A}$ determined by real-time quantitative RT–PCR in cultured HuH-7 cells in combination with the cGKII expression vector (+) or the empty vector (–). Data are mean (bars) ± S.E.M. (error bars) of six wells/group. (#) $P < 0.01$, significant stimulation by Sox9. (*) $P < 0.01$, significant inhibition by cGKII.

cytoplasm. Addition of leptomycin B, an inhibitor of CRM-1-dependent nuclear export (Gasca et al. 2002), failed to restore the altered localization of Sox9, suggesting that cGKII attenuated the nuclear entry of Sox9 rather than enhanced its export from the nucleus. As cGKII also altered the subcellular localization of phosphorylation-deficient Sox9 ($Sox9^{S181A}$) in a similar manner, phosphorylation at S181 was shown to be dispensable for this regulatory mechanism. Interestingly, the subcellular localization of Sox5 and Sox6, critical partners of Sox9, was not affected by cGKII (Fig. 6A). The altered subcellular localization of Sox9 was confirmed by an immunoblot analysis: the cGKII cotransfection increased the Sox9 protein level in the cytoplasmic fraction although it decreased that in the nuclear fraction (Fig. 6B). To determine whether or not the attenuated Sox9 signaling by cGKII was attributable to the decreased nuclear entry of Sox9, we fused Sox9 with SV40-derived nuclear localization signal (Sox9-3xNLS), thereby forcing Sox9 to localize in the nucleus. The cGKII cotransfection was unable to keep the Sox9 in the cytoplasm in HeLa cells (Fig. 6C, left panel). In this condition, the inhibitory effect of cGKII on the Sox9-induced COL2 expression was greatly alleviated, indicating that cGKII attenuated the Sox9 function mainly, if not exclusively, by interfering with its nuclear entry (Fig. 6C, right panel). To further examine the change of Sox9 subcellular localization in the KMI chondrocytes, we adenovirally transduced cultured primary chondrocytes from wild-type and KMI growth plates with GFP-Sox9. Treatment with the cGMP analog 8-bromo-cGMP inhibited nuclear entry of Sox9 in wild-type cells, whereas it did not in KMI cells. CNP, a putative upstream molecule of cGKII, showed a similar effect on the Sox9 subcellular localization in wild-type cells, but not in KMI cells (Fig. 6D). Finally, we examined the effects of the silencing of Sox9 through RNA interference (RNAi) on the cultured growth plate chondrocytes from KMI (Fig. 6E). The impaired differentiation of KMI chondrocytes determined by the ALP staining and the COL10 mRNA level was reversed by the retrovirus-mediated introduction of Sox9 RNAi. Taken together, these results demonstrate that

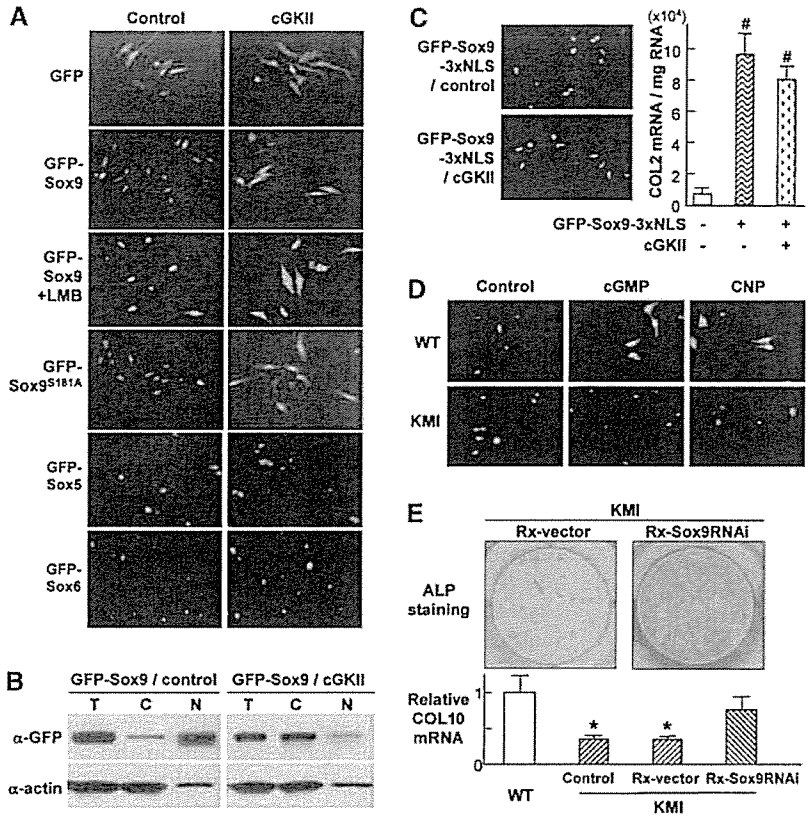

Figure 6. Regulation of Sox9 function and subcellular localization by cGKII. (*A*) Fluorescent images of HeLa cells cotransfected with cGKII and Sox9, Sox5, or Sox6. Cells were transfected with plasmids encoding GFP, GFP-tagged Sox9 (GFP-Sox9) in the presence and absence of a nuclear export inhibitor leptomycin (LMB; 2 ng/mL), and GFP-Sox9^{S181A}, GFP-Sox5, and GFP-Sox6 in combination with the cGKII expression vector or the empty vector (control). (*B*) Subcellular localization of Sox9 in HeLa cells by immunoblotting. GFP-Sox9 was cotransfected with the cGKII expression vector or the empty vector (control). The Sox9 protein levels in the total cell lysate (T), cytoplasmic fraction (C), and nuclear fraction (N) were determined by immunoblotting with an anti-GFP antibody (α-GFP). Blottings with anti-β-actin (α-actin) were used as loading controls. (*C, left*) Fluorescent images of HeLa cells transfected with the nuclear-localizing Sox9 vector. Three tandem repeats of SV40-derived nuclear localizing signal (NLS) were introduced into the GFP-Sox9 vector (GFP-Sox9-3xNLS). Cells were transfected with the GFP-Sox9-3xNLS in combination with the cGKII expressing vector or the empty vector (control). (*Right*) Induction of COL2 mRNA by the GFP-Sox9-3xNLS transfection determined by real-time quantitative RT–PCR in cultured HuH-7 cells cotransfected with the cGKII expression vector (+) or the empty vector (–). Data are mean (bars) ± S.E.M. (error bars) of six wells/group. (#) $P < 0.01$, significant stimulation by GFP-Sox9-3xNLS. (*D*) Fluorescent images of wild-type (WT) and KMI growth plate chondrocytes transduced with GFP-Sox9 adenovirus vector. Primary chondrocytes were cultured in the presence and absence of 8-Bromo-cGMP (100 μM) or CNP (100 nM). (*E*) Effects of the silencing of Sox9 through RNAi on the ALP staining and the COL10 mRNA level determined by real-time quantitative RT–PCR in the KMI chondrocyte culture for 21 and 28 d, respectively. The Sox9 RNAi was introduced into KMI chondrocytes using an retrovirus vector carrying the Sox9 RNAi gene (Rx-Sox9RNAi). Retrovirus vector without the the Sox9 RNAi gene (Rx-vector) was used as control. Data are mean (bars) ± S.E.M. (error bars) of six wells/group. (*) $P < 0.01$ vs. wild type.

the cGKII dysfunction in KMI impaired the hypertrophic differentiation of chondrocytes through enhancement of the Sox9 signaling.

Discussion

Although postproliferative chondrocytes immediately undergo hypertrophic differentiation during endochondral ossification, little has been known about the molecular mechanism that couples the cessation of proliferation and the start of hypertrophy. The present study for the first time identified a novel role of cGKII as a molecular switch for the coupling. The study began with the identification of a mutation in the *cGKII* gene causing the longitudinal growth retardation of a rat dwarf model, KMI. Analyses of the growth plate and the bone fracture callus of KMI revealed that the cessation of proliferation and the start of hypertrophic differentiation of chondrocytes were dissociated. Cultures of KMI chondrocytes confirmed that the cGKII dysfunction impairs the synchronized switching from proliferation to hypertrophic differentiation. This KMI chondrocyte abnormality may be due to the sustained activity of Sox9, as cGKII was shown to function as an attenuator of Sox9 mainly by inhibiting its nuclear entry.

Physiological function of cGKII

In mammalian cells, at least three receptors for cGMP are present, that is, cGMP-regulated PDEs, cyclic nucleotide-gated cation channels, and cGKs (Ruth 1999). Mammalian cGKs exist as two isoforms, cGKI and cGKII (Hofmann et al. 2000). Whereas the cGKI is expressed at high levels in all types of smooth muscle, platelets, and cerebellar cells, cGKII is expressed in the intestinal mucosa, juxtaglomerular cells of the kidney, and chondrocytes (Pfeifer et al. 1996). The widespread expression of cGKs is mirrored by the diversity of their functions, which establish these enzymes as major mediators of the cGMP signaling cascade. Studies on the ablation of the genes disclosed the pivotal tasks of these enzymes under in vivo conditions (Pfeifer et al. 1996, 1998). *cGKII*-deficient (*cGKII*$^{-/-}$) mice were reported to develop dwarfism postnatally, which was caused by a severe defect in en-

dochondral ossification at the growth plates (Pfeifer et al. 1996). Although the phenotypes were quite similar to those of KMI, the abnormal population of chondrocytes in the *cGKII*$^{-/-}$ growth plate was though to constitute a hypertrophic zone with patches of nonhypertrophic cells intermingled with hypertrophic chondrocytes. Our more detailed histological examination of the KMI growth plate clearly showed that these cells were postmitotic but nonhypertrophic chondrocytes. Further examinations of the *cGKII*$^{-/-}$ growth plate would probably reveal similar findings confirming the unique role of cGKII in the coupling of chondrocyte proliferation and differentiation.

cGKII and CNP signaling

CNP is a positive regulator of endochondral ossification through the intracellular accumulation of cGMP, which activates different signaling mediators such as cyclic nucleotide phosphodiesterases, cGMP-regulated ion channels, and cGKs (Fowkes and McArdle 2000). Among them, cGKII is reported to play a critical role in the CNP action on endochondral ossification, because targeted expression of CNP in the growth plate chondrocytes failed to rescue the skeletal defect of *cGKII*$^{-/-}$ mice (Miyazawa et al. 2002). This notion was supported by the present findings that CNP neither reverses the impaired differentiation (Fig. 4D) nor inhibits the Sox9 nuclear entry (Fig. 6D) in cultured KMI chondrocytes. However, there is a marked difference between *CNP*$^{-/-}$ and *cGKII*$^{-/-}$ mice in the histology of the growth plate (Pfeifer et al. 1996; Chusho et al. 2001): the growth plate of the former is reduced in height with the chondrocytes arranged in a regular columnar array, whereas that of the latter is increased in height. This may indicate the involvement of other signaling pathway(s) in the CNP-mediated endochondral ossification. In fact, a recent report showed that targeted overexpression of CNP in chondrocytes prevented the shortening of achondroplastic bones through inhibition of the mitogen-activated protein (MAP) kinase pathway of activated fibroblast growth factor receptor 3 signaling in the growth plate (Yasoda et al. 2004). In addition, the possibility of the involvement of cGKI cannot be ruled out, although no skeletal abnormality has been reported in *cGKI*$^{-/-}$ mice (Pfeifer et al. 1998). It would be helpful to investigate whether mice doubly deficient for *cGKI* and *cGKII* mimic the phenotype of *CNP*$^{-/-}$ mice.

cGKII and PTH/PTHrP signaling

Targeted expression of a constitutively active PTH/PTHrP receptor delays endochondral ossification through ligand-independent constitutive cAMP accumulation and the subsequent cAMP-dependent protein kinase (cAK) activation (Schipani et al. 1997). The growth plate histology of the transgenic mice expressing a constitutively active PTH/PTHrP receptor is characterized by the irregular and broadened zone lacking the COL10 expression, which is similar to that of KMI and *cGKII*$^{-/-}$ mice. In the present study, however, neither the expression levels of PTHrP and PTH/PTHrP receptor nor the cAMP accumulation by PTH stimulation was enhanced in the cultured KMI chondrocytes. It is therefore speculated that the cGKII and PTH/PTHrP/cAK signaling pathways independently coordinate to control the rate of chondrocytic differentiation as an accelerator and a decelerator, respectively.

Regulation of Sox9 actions by cGKII

In addition to its essential roles in early mesenchymal condensation and development of premature chondrocytes, Sox9 is reported to prevent hypertrophic differentiation of chondrocytes (de Crombrugghe et al. 2001; Akiyama et al. 2002). Although the present findings demonstrated that cGKII maintains the hypertrophy by attenuating the Sox9 activity, the molecular mechanism remains to be clarified in more detail. The fact that cGKII lacking the kinase activity did not suppress the Sox9 function suggests that phosphorylation by cGKII is required for the regulation of Sox9 activity. Although cGKII enhanced the phosphorylation of Sox9 at S181, which has been known to be a phosphorylation target for PKA signaling (Huang et al. 2000), the attenuation of Sox9 by cGKII was not dependent on the phosphorylation at this site (Fig. 5D). Along with S181, Ser 64 (S64) is also known to be a phosphorylation target for PKA (Huang et al. 2000); however, this site does not contain the consensus sequence for phosphorylation by cGKII (RRXS/TX). In addition, cGKII suppressed the COL2 induction in cultured HuH-7 cells transfected with a phosphorylation-deficient Sox9 vector at this site ($Sox9^{S64A}$) as with the wild-type Sox9 or $Sox9^{S181A}$ (data not shown), indicating that the direct phosphorylation of Sox9 is dispensable for its attenuation by cGKII. Several lines of evidence indicated that transcriptional factors of the Sox family are regulated by subcellular distribution (Sudbeck and Scherer 1997; Harley et al. 2003). The present findings also indicate that cGKII attenuates the Sox9 function at least in part by inhibiting its nuclear entry. Because this cGKII effect was seen in cells transfected with the phosphorylation-deficient Sox9, the phosphorylation and the nuclear entry of Sox9 were independent, although both were affected by cGKII. Hence, there seem to be other phosphorylation target molecules that mediate cGKII signaling. Sox genes including Sox9 require partner molecules that enhance or suppress transcriptional activities. For example, Sox5 and Sox6 cooperatively work with Sox9 and activate several cartilage matrix genes (Lefebvre and deCrombugghe 1998); however, our computer search found no amino acid sequence in Sox5 or Sox6 for a cGKII phosphorylation site like S181 in Sox9. Furthermore, our results revealed that their subcellular localizations were not altered by cGKII (Fig. 6A), suggesting that it is unlikely that Sox5 and Sox6 are the direct target of cGKII. It was recently revealed that the dimerization of Sox9 is critical for its several target genes. Sox9 contains a dimerization domain and binds

cooperatively as a dimer in the presence of the DNA enhancer element in genes involved in chondrocyte differentiation, such as COL9, COL11, and CD-Rap (Sock et al. 2003). Because in vitro-transcripted Sox9 was unable to form a DNA-dependent dimer (Lefebvre et al. 1998), there must be cofactor(s) that mediate the dimerization of Sox9. Although phosphorylation of these partner molecules remains to be resolved, one of these molecules might be a direct or indirect phosphorylational target of cGKII.

cGKII, a molecular switch from proliferation to hypertrophic differentiation of chondrocytes, could be a novel therapeutic target for disorders of skeletal growth and regeneration. Because cGKII is an intracellular kinase, we are planning to apply the gene transfer system that we are now intensively working on (Itaka et al. 2002) for bone regenerative medicine. Otherwise, a small compound that modulates cGKII activity in vivo would be a good candidate for a new therapeutic drug.

Materials and methods

Genetic mapping

Heterozygous (BN × KMI-*mri/mri*) F1 rats were backcrossed to KMI-*mri/mri* homozygous rats to obtain backcross progeny (241 homozygotes among 475 backcross progeny). Animals were genotyped with SSLP markers (Rat Genome Database, http://rgd.mcw.edu). The segregation patterns of the markers were analyzed with the Map Manager computer program. The rat–mouse–human comparative map was constructed based on the data obtained from the following databases: RatMap (http://ratmap.gen.gu.se), Mouse Genome Informatics (http://www.informatics.jax.org), and University of California at Santa Cruz Genome Browser (http://genome.ucsc.edu).

Positional candidate cloning of the mri *locus*

Total RNA from rat intestine was prepared and subjected to RT–PCR using specific primers to amplify overlapping products that cover the coding region of the rat *cGKII* gene. Genomic DNA was isolated from rat liver, and interexon PCR was carried out with primers as follows: 5′-CTTATCACAGACGCCCTGAATAAGAAC-3′ and 5′-CACTTCCAAGCAGTCAATAATCTTGGT-3′. The amplified pruducts were sequenced using ABI PRISM 310 Genetic Analyzer (Applied Biosystems).

Animals were genotyped with primers as follows: common forward, 5′-TGTATTTTCCCGTCCGACAC-3′; wild-type reverse, 5′-TCCTTCGATGCCACCGTAAT-3′; and KMI reverse, 5′-CAGAGTACGCTAGGTTCCAAGG-3′.

In vitro kinase assay

Wild-type and KMI brain extracts (40 µg) were prepared using T-PER (Pierce). Kinase activity was determined by the phosphorylation of biotinylated substrate peptide (250 µM, Biotynyl-RKISASEFDRPLR-OH, Bachem) in the presence of PKI (2 µM, Sigma) and 8-bromo-cGMP (100 µM) for 30 min at 30°C using the AUSA Universal Protein Kinase Assay Kit (TRANSBIO).

Histological analysis

Tissues were fixed in 4% paraformaldehyde and decalcified in 10% EDTA, if necessary, then embedded in paraffin and cut into 6-µm sections. Hematoxylin eosin (HE) staining and von Kossa staining were done according to the standard procedure. For enzyme histochemistry, ALP was visualized using X-phosphate and NBT (Roche). For immunohistochemistry, sections were incubated with primary antibody at 4°C overnight. Primary antibodies were purchased from Santa Cruz Biotechnology. Signal was detected with HRP-conjugated secondary antibody. For fluorescent visualization, a secondary antibody conjugated with Alexa 488 (Molecular Probes) was used.

In vivo BrdU labeling

Animals were injected intraperitoneally with BrdU (Sigma), 25 µg per gram body weight 2 h prior to sacrifice. Incorporated BrdU was detected using a BrdU immunostaining kit (Roche).

Fracture model

A fracture was generated on the mid-part of the tibiae of 10-week-old animals (n = 10/group). Animals were sacrificed 2 wk after the surgery. Fracture callus was quantitated as described (Shimoaka et al. 2004).

Analysis of growth plate chondrocytes

Growth plate chondrocytes were isolated from the tibiae of 4-week-old animals as described (Klaus et al. 1991). Cells were cultured in Dubecco's Modified Eagle's Medium (DMEM) supplemented with 10% fetal bovine serum (FBS). For cellular proliferation assay, 1×10^5 cells were plated on a 6-cm dish and counted after designated periods. To assess differentiation, cells were incubated for a designated period with hBMP-2 (100 ng/mL) and CNP (100 nM) when needed. They were stained for ALP, and ALP activity was quantitated as described (Shimoaka et al. 2004). RNA was isolated and subjected to semiquantitative RT–PCR analysis. Primer information will be provided upon request.

Plasmids and viral vectors

cDNA of rat cGKII (nucleotides 48–2333) was ligated into pcDNA4HisA (Invitrogen). A PCR-amplified fragment (nucleotides 48–1403) was used to construct the cGKII-Δkinase vector. Full-length human Sox5, Sox6, and Sox9 were ligated into pEGFPC1 (Clontech) to generate GFP-tagged plasmids. To create amino acid change (S181A and S64A), GFP-Sox9 plasmid was subjected to site-directed mutagenesis using the inverse PCR technique. To construct nuclear-localizing GFP-Sox9 vector (Sox9-3xNLS), a three-tandem repeat of SV40-derived nuclear localizing signal was ligated into pEGFPC1. All constructs were verified by sequencing. cGKII and GFP-Sox9 adenovirus vectors were constructed using the Adeno-X Expression System (BD Biosciences), according to the manufacturer's protocol. RNAi sequence was designed for the rat *Sox9* gene (nucleotides 190–219, AB073720.1) as described (Kawasaki and Taira 2003) and ligated into piGENEtRNA vector (iGENE Therapeutics). RNAi sequence combined with promotor was then inserted into pMx vector (Kitamura 1998), and retroviral vector was generated using plat-E cells (Morita et al. 2000).

Cell culture and transient transfection

HuH-7 and HeLa were cultured in DMEM supplemented with 10% FBS. ATDC5 was maintained as described (Shukunami et al. 1996). For transient transfection, a total of 1 µg plasmid DNA was transfected using FuGENE6 (Roche). In cotransfection, all

plasmids were added in an equal ratio. 8-bromo-cGMP (100 μM, BioMol) was added 4 h after transfection. Total RNA was isolated 72 h after transfection and subjected to real-time PCR analysis. For fluorescent detection, HeLa cells were transiently transfected and fluorescent images were taken 24 h after transfection. Cells were incubated with 2.5 ng/mL leptomycin B (Sigma) for the last 3 h when required. For the differentiation assay, ATDC5 cells were transiently cotransfected with Sox9 vector (3 μg) and a designated amount of cGKII vector. Two days after transfection, a three-dimensional alginate beads culture was performed as described (Seki et al. 2003) in the presence of 8-bromo-cGMP (100 μM) and ITS supplement (Sigma). RNA was isolated 7 d after transfection and subjected to real-time PCR analysis.

Western blotting

Samples were prepared using M-PER (Pierce) or NE-PER (Pierce) supplemented with Na_3Vo_4 (2 mM), NaF (10 mM), and aprotinin (10 μg/mL) following the manufacturer's protocol. An equal amount (20 μg) of protein was subjected to SDS-PAGE, and transferred onto PVDF membranes. Anti-EGFP antibody (Clontech) and anti-Sox9 (pS^{181}) phosphospecific antibody (BioSource) were used. The membrane was incubated with HRP-conjugated secondary antibody (Promega). Immunoreactive proteins were visualized by ECL (Amersham).

PTH-induced cAMP accumulation

Cells were preincubated with 8-bromo-cGMP (100 μM) for 30 min, then challenged with increasing concentrations of PTH (Sigma) and incubated at 37°C for 30 min in the presence of IBMX (2 mM). Intercellular cAMP was measured using the cAMP Biotrack EIA system (Amersham) following the manufacturer's protocol.

Statistical analysis

Means of groups were compared by ANOVA, and significance of differences was determined by post-hoc testing with Bonferroni's method.

Acknowledgments

We thank Drs. Benoit de Crombrugghe, Sakae Tanaka, Yasuo Terauchi, and Takashi Kadowaki for critical discussions. We also thank Reiko Yamaguchi, Mizue Ikeuchi, and Misako Namae for their excellent technical help. This work was supported by Grants-in-Aid for Scientific Research from the Japanese Ministry of Education, Culture, Sports, Science and Technology (#14657359 and #15591566).

References

Akiyama, H., Chaboissier, M.C., Martin, J.F., Schedl, A., and de Crombrugghe, B. 2002. The transcription factor Sox9 has essential roles in successive steps of the chondrocyte differentiation pathway and is required for expression of Sox5 and Sox6. *Genes & Dev.* **16:** 2813–2828.

Chung, U. and Kronenberg, H. 2000. Role of parathyroid hormone-related protein and indian hedgehog in skeletal development. In *Skeletal growth factors* (ed. C. Canalis), pp. 355–364. Lippincott Willams & Wilkins, Philadelphia.

Chusho, H., Tamura, N., Ogawa, Y., Yasoda, A., Suda, M., Miyazawa, T., Nakamura, K., Nakao, K., Kurihara, T., Komatsu, Y., et al. 2001. Dwarfism and early death in mice lacking C-type natriuretic peptide. *Proc. Natl. Acad. Sci.* **98:** 4016–4021.

Daluiski, A., Engstrand, T., Bahamonde, M.E., Gamer, L.W., Agius, E., Stevenson, S.L., Cox, K., Rosen, V., and Lyons, K.M. 2001. Bone morphogenetic protein-3 is a negative regulator of bone density. *Nat. Genet.* **27:** 84–88.

de Crombrugghe, B., Lefebvre, V., and Nakashima, K. 2001. Regulatory mechanisms in the pathways of cartilage and bone formation. *Curr. Opin. Cell Biol.* **13:** 721–727.

Fowkes, R.C. and McArdle, C.A. 2000. C-type natriuretic peptide: An important neuroendocrine regulator? *Trends Endocrinol. Metab.* **11:** 333–338.

Gasca, S., Canizares, J., De Santa Barbara, P., Mejean, C., Poulat, F., Berta, P., and Boizet-Bonhoure, B. 2002. A nuclear export signal within the high mobility group domain regulates the nucleocytoplasmic translocation of SOX9 during sexual determination. *Proc. Natl. Acad. Sci.* **99:** 11199–11204.

Harley, V.R., Clarkson, M.J., and Argentaro, A. 2003. The molecular action and regulation of the testis-determining factors, SRY (sex-determining region on the Y chromosome) and SOX9 [SRY-related high-mobility group (HMG) box 9]. *Endocr. Rev.* **24:** 466–487.

Hofmann, F. 1995. cGMP-dependent protein kinase (vertebrates). In *The protein kinase factsbook* (eds. G. Hardie and S. Hanks), pp. 73–76. Academic Press, San Diego.

Hofmann, F., Ammendola, A., and Schlossmann, J. 2000. Rising behind NO: cGMP-dependent protein kinases. *J. Cell Sci.* **113:** 1671–1676.

Huang, W., Zhou, X., Lefebvre, V., and de Crombrugghe, B. 2000. Phosphorylation of SOX9 by cyclic AMP-dependent protein kinase A enhances SOX9's ability to transactivate a Col2a1 chondrocyte-specific enhancer. *Mol. Cell Biol.* **20:** 4149–4158.

Huang, W., Chung, U.I., Kronenberg, H.M., and de Crombrugghe, B. 2001. The chondrogenic transcription factor Sox9 is a target of signaling by the parathyroid hormone-related peptide in the growth plate of endochondral bones. *Proc. Natl. Acad. Sci.* **98:** 160–165.

Itaka, K., Harada, A., Nakamura, K., Kawaguchi, H., and Kataoka, K. 2002. Evaluation by fluorescence resonance energy transfer of the stability of nonviral gene delivery vectors under physiological conditions. *Biomacromolecules* **3:** 841–845.

Kawasaki, H. and Taira, K. 2003. Short hairpin type of dsRNAs that are controlled by tRNA(Val) promoter significantly induce RNAi-mediated gene silencing in the cytoplasm of human cells. *Nucleic Acids Res.* **31:** 700–707.

Kitamura, T. 1998. New experimental approaches in retrovirus-mediated expression screening. *Int. J. Hematol.* **67:** 351–359.

Klaus, G., Merke, J., Eing, H., Hugel, U., Milde, P., Reichel, H., Ritz, E., and Mehls, O. 1991. 1,25(OH)2D3 receptor regulation and 1,25(OH)2D3 effects in primary cultures of growth cartilage cells of the rat. *Calcif. Tissue Int.* **49:** 340–348.

Kronenberg, H.M. 2003. Developmental regulation of the growth plate. *Nature* **423:** 332–336.

Lefebvre, V., Li, P., and de Crombrugghe, B. 1998. A new long form of Sox5 (L-Sox5), Sox6 and Sox9 are coexpressed in chondrogenesis and cooperatively activate the type II collagen gene. *EMBO J.* **17:** 5718–5733.

Miyazawa, T., Ogawa, Y., Chusho, H., Yasoda, A., Tamura, N., Komatsu, Y., Pfeifer, A., Hofmann, F., and Nakao, K. 2002. Cyclic GMP-dependent protein kinase II plays a critical role in C-type natriuretic peptide-mediated endochondral ossification. *Endocrinology* **143:** 3604–3610.

Morita, S., Kojima, T., and Kitamura, T. 2000. Plat-E: An effi-

cient and stable system for transient packaging of retroviruses. *Gene Ther.* **7:** 1063–1066.

Pfeifer, A., Aszodi, A., Seidler, U., Ruth, P., Hofmann, F., and Fassler, R. 1996. Intestinal secretory defects and dwarfism in mice lacking cGMP-dependent protein kinase II. *Science* **274:** 2082–2086.

Pfeifer, A., Klatt, P., Massberg, S., Ny, L., Sausbier, M., Hirneiss, C., Wang, G.X., Korth, M., Aszodi, A., Andersson, K.E., et al. 1998. Defective smooth muscle regulation in cGMP kinase I-deficient mice. *EMBO J.* **17:** 3045–3041.

Ruth, P. 1999. Cyclic GMP-dependent protein kinases: Understanding in vivo functions by gene targeting. *Pharmacol. Ther.* **82:** 355–372.

Schipani, E., Lanske, B., Hunzelman, J., Luz, A., Kovacs, C.S., Lee, K., Pirro, A., Kronenberg, H.M., and Juppner, H. 1997. Targeted expression of constitutively active receptors for parathyroid hormone and parathyroid hormone-related peptide delays endochondral bone formation and rescues mice that lack parathyroid hormone-related peptide. *Proc. Natl. Acad. Sci.* **94:** 13689–13694.

Seki, K., Fujimori, T., Savagner, P., Hata, A., Aikawa, T., Ogata, N., Nabeshima, Y., and Kaechoong, L. 2003. Mouse Snail family transcription repressors regulate chondrocyte, extracellular matrix, type II collagen, and aggrecan. *J. Biol. Chem.* **278:** 41862–41870.

Serizawa, N. 1993. Initial characterization of a new miniature animal model in the rat: Studies on anatomy, pituitary hormones and GH mRNA in miniature rat Ishikawa. *Nippon Naibunpi Gakkai Zasshi* **69:** 33–45.

Shimoaka, T., Kamekura, S., Chikuda, H., Hoshi, K., Chung, U.I., Akune, T., Maruyama, Z., Komori, T., Matsumoto, M., Ogawa, W., et al. 2004. Impairment of bone healing by insulin receptor substrate-1 deficiency. *J. Biol. Chem.* **279:** 15314–15322.

Shukunami, C., Shigeno, C., Atsumi, T., Ishizeki, K., Suzuki, F., and Hiraki, Y. 1996. Chondrogenic differentiation of clonal mouse embryonic cell line ATDC5 in vitro: Differentiation-dependent gene expression of parathyroid hormone (PTH)/PTH-related peptide receptor. *J. Cell Biol.* **133:** 457–468.

Sock, E., Pagon, R.A., Keymolen, K., Lissens, W., Wegner, M., and Scherer, G. 2003. Loss of DNA-dependent dimerization of the transcription factor SOX9 as a cause for campomelic dysplasia. *Hum. Mol. Genet.* **12:** 1439–1447.

Sorrentino, V., Pepperkok, R., Davis, R.L., Ansorge, W., and Philipson, L. 1990. Cell proliferation inhibited by MyoD1 independently of myogenic differentiation. *Nature* **345:** 813–815.

Stewart, M.C., Kadlcek, R.M., Robbins, P.D., MacLeod, J.N., and Ballock, R.T. 2004. Expression and activity of the CDK inhibitor p57Kip2 in chondrocytes undergoing hypertrophic differentiation. *J. Bone Miner. Res.* **19:** 123–132.

Sudbeck, P. and Scherer, G. 1997. Two independent nuclear localization signals are present in the DNA-binding high-mobility group domains of SRY and SOX9. *J. Biol. Chem.* **272:** 27848–27852.

Tao, H. and Umek, R.M. 2000. C/EBPα is required to maintain postmitotic growth arrest in adipocytes. *DNA Cell Biol.* **19:** 9–18.

Umek, R.M., Friedman, A.D., and McKnight, S.L. 1991. CCAAT-enhancer binding protein: A component of a differentiation switch. *Science* **251:** 288–292.

Yan, Y., Frisen, J., Lee, M.H., Massague, J., and Barbacid, M. 1997. Ablation of the CDK inhibitor p57Kip2 results in increased apoptosis and delayed differentiation during mouse development. *Genes & Dev.* **11:** 973–983.

Yasoda, A., Komatsu, Y., Chusho, H., Miyazawa, T., Ozasa, A., Miura, M., Kurihara, T., Rogi, T., Tanaka, S., Suda, M., et al. 2004. Overexpression of CNP in chondrocytes rescues achondroplasia through a MAPK-dependent pathway. *Nat. Med.* **10:** 80–86.

Stimulatory G protein directly regulates hypertrophic differentiation of growth plate cartilage in vivo

Murat Bastepe, Lee S. Weinstein, Naoshi Ogata, Hiroshi Kawaguchi, Harald Jüppner, Henry M. Kronenberg, and Ung-il Chung

PNAS 2004;101;14794-14799; originally published online Sep 30, 2004;
doi:10.1073/pnas.0405091101

Stimulatory G protein directly regulates hypertrophic differentiation of growth plate cartilage *in vivo*

Murat Bastepe*, Lee S. Weinstein†, Naoshi Ogata‡, Hiroshi Kawaguchi‡, Harald Jüppner*, Henry M. Kronenberg*, and Ung-il Chung‡§

*Endocrine Unit, Massachusetts General Hospital and Harvard Medical School, Boston, MA 02114; †Metabolic Diseases Branch, National Institute of Diabetes and Digestive and Kidney Diseases, National Institutes of Health, Bethesda, MD 20892; and ‡Division of Tissue Engineering, University of Tokyo Hospital, Tokyo 113-8655, Japan

Edited by Lutz Birnbaumer, National Institutes of Health, Research Triangle Park, NC, and approved September 7, 2004 (received for review July 14, 2004)

Stimulatory heterotrimeric G protein (Gs) transduces signals from various cell-surface receptors to adenylyl cyclases, which generate cAMP. The α subunit of Gs (Gsα) is encoded by *GNAS* (*Gnas* in mice), and heterozygous Gsα inactivating mutations lead to Albright hereditary osteodystrophy. The *in vivo* role of Gsα in skeletogenesis is largely unknown, because of early embryonic lethality of mice with disruption of *Gnas* exon 2 ($Gnas^{E2-/E2-}$) and the absence of easily detectable phenotypes in growth plate chondrocytes of heterozygous mutant mice ($Gnas^{+/E2-}$). We generated chimeric mice containing wild-type cells and either $Gnas^{E2-/E2-}$ or $Gnas^{+/E2-}$ cells. $Gnas^{E2-/E2-}$ chondrocytes phenocopied *PTH/PTHrP receptor* (*PPR*)$^{-/-}$ cells by prematurely undergoing hypertrophy. Introduction of a transgene expressing Gsα, one of several gene products that include *Gnas* exon 2, into $Gnas^{E2-/E2-}$ cells prevented premature hypertrophy. Gsα mRNA expression detected by real-time RT-PCR analysis was reduced to approximately half that of the wild-type in both paternal and maternal $Gnas^{+/E2-}$ growth plate chondrocytes, indicating biallelic expression of Gsα in these cells. Hypertrophy of $Gnas^{+/E2-}$ chondrocytes was modestly but significantly premature in chimeric growth plates of mice containing wild-type and $Gnas^{+/E2-}$ cells. These data suggest that Gsα is the primary mediator of the actions of PPR in growth plate chondrocytes and that there is haploinsufficiency of Gsα signaling in $Gnas^{+/E2-}$ chondrocytes.

Parathyroid hormone (PTH)-related protein (PTHrP) is a paracrine factor important for regulation of chondrocyte differentiation during endochondral bone formation. Actions of PTHrP are mediated through the PTH/PTHrP receptor (PPR), which can couple to both stimulatory heterotrimeric G protein (Gs) (which activates adenylyl cyclase) and Gq/11 (which activates phospholipase C) in cultured cells (1, 2). Growth plate chondrocytes in $PTHrP^{-/-}$ or $PPR^{-/-}$ mice show accelerated hypertrophy (3, 4). In contrast, mice carrying a mutant PPR selectively deficient in signaling through Gq show a mild delay in hypertrophy of growth plate chondrocytes (5). Thus, opposing actions of Gs and Gq signaling pathways may be required for normal endochondral bone formation.

The α subunit of Gs (Gsα) is encoded by *GNAS* (*Gnas* in mice), a complex gene locus leading to multiple imprinted transcripts through the use of different first exons and promoters (6). Heterozygous mutations in *GNAS* exons 1–13 encoding Gsα (*Gnas* exons 1–12 in mice, because the intron between exons 9 and 10 is absent in mice) are associated with skeletal defects as part of a constellation of physical features termed Albright hereditary osteodystrophy (AHO), including short stature and brachydactyly (6, 7). In some patients, the same *GNAS* mutations additionally lead to resistance to some, but not all, hormones that act via Gsα, including PTH and thyroid stimulating hormone, a condition termed pseudohypoparathyroidism (PHP) type Ia (6–8). Whereas maternal inheritance of a Gsα mutation leads to PHP type Ia, paternal transmission of the same mutation results in pseudopseudohypoparathyroidism (PPHP), a disorder characterized by AHO in the absence of hormone resistance. Consistent with this imprinted mode of inheritance of hormone resistance, Gsα expression occurs predominantly from the maternal allele in certain human tissues, including the thyroid gland (9–11), the ovary (9), and the pituitary gland (12). In the renal cortex, there is evidence for both biallelic (13) and maternal expression of Gsα (14). AHO, unlike hormone resistance, develops after both paternal and maternal transmission of Gsα mutations. These mutations lead to $\approx$50% reduction of Gsα protein level/activity in erythrocytes and skin fibroblasts of patients with PHP type Ia and PPHP. It has therefore been hypothesized that haploinsufficiency of Gs signaling in various tissues may be responsible for the development of the AHO phenotype (6, 15).

Consistent with the maternal inheritance of hormonal resistance in PHP type Ia, mice heterozygous for disruption of maternal *Gnas* exon 2 ($Gnas^{matE2-/+}$), but not those heterozygous for disruption of paternal *Gnas* exon 2 ($Gnas^{+/patE2-}$), have reduced Gsα levels in renal cortex along with PTH resistance (16). Also consistent with the short stature observed in AHO, both $Gnas^{matE2-/+}$ and $Gnas^{+/patE2-}$ mice are shorter than wild-type littermates. However, the growth plates of these animals appear normal, making it difficult to assess whether the short stature is due to deficiency of Gsα in growth plate cartilage or due to systemic effects. Hence, although the mouse model with disrupted *Gnas* exon 2 provided important insights into the mechanisms underlying hormonal resistance in PHP type Ia, it did not explain the skeletal phenotypes of AHO. Moreover, homozygous disruption of *Gnas* exon 2 leads to early embryonic lethality during the postimplantation stage of development, and it has therefore remained unclear whether total loss of Gsα in the growth plate results in a phenotype similar to that observed in $PPR^{-/-}$ or $PTHrP^{-/-}$ mice or one that is unique, perhaps due to disruption of other undefined regulatory pathways that also use Gsα signaling in the growth plate. Furthermore, XLαs, a large variant of Gsα with a distinct amino terminus encoded by transcripts using a unique first exon, has "Gs-like" signaling properties *in vitro* (6, 17, 18), and it thus has to be clarified whether this paternally expressed protein may have a distinct role in the growth plate.

To better evaluate *in vivo* roles of Gsα in endochondral bone formation as well as to address whether haploinsufficiency of Gsα signaling contributes to the AHO skeletal phenotype, we generated chimeric mice containing both wild-type cells and cells with a null mutation in the *Gnas* exon 2, and compared both cell types side by side *in vivo*.

Methods

Generation of Embryonic Stem (ES) Cell Lines *de Novo*. ES cells were generated as described in ref. 19. To generate $Gnas^{+/patE2-}$ and

This paper was submitted directly (Track II) to the PNAS office.

Abbreviations: AHO, Albright hereditary osteodystrophy; CMV, cytomegalovirus; E*n*, embryonic day *n*; ES, embryonic stem; HA, hemagglutinin; H&E, hematoxylin/eosin; PTH, parathyroid hormone; PTHrP, PTH-related protein; PPR, PTH/PTHrP receptor.

§To whom correspondence should be addressed at: Division of Tissue Engineering, University of Tokyo Hospital, 7-3-1 Hongo, Bunkyoku, Tokyo 113-8655, Japan. E-mail: teiy-ort@h.u-tokyo.ac.jp.

www.pnas.org/cgi/doi/10.1073/pnas.0405091101

$Gnas^{matE2-/+}$ ES cell lines, male and female $Gnas^{+/E2-}$ mice in a CD1 background were mated with wild-type C57BL/6 female and male mice, respectively, for blastocyst collection. To generate $Gnas^{E2-/E2-}$ ES cell lines, $Gnas^{+/E2-}$ mice in a CD1-C57BL/6 F_1 hybrid background (16) were mated with each other for blastocyst collection. ES cells homozygous for the null mutation in the PPR gene were isolated as described in ref. 20.

Stable Transfection of $Gnas^{E2-/E2-}$ ES Cells with a Plasmid Encoding Gsα. Rat Gsα cDNA with a hemagglutinin (HA) tag (a generous gift from A. Federman, University of California, San Francisco) was subcloned into *Xho*I–*Hin*dIII sites of the pcDNA3.1/hyg(−) vector (Invitrogen), which uses the cytomegalovirus (CMV) promoter to drive expression. We call the resultant expression vector pCMV-rGsα; note that rat and human Gsα proteins are virtually identical with only a single amino acid difference (residue 139 is asparagine in rat and aspartic acid in human). The expression vector was linearized with *Mfe*I. $Gnas^{E2-/E2-}$ ES cells were plated onto a hygromycin-resistant feeder layer, and they were transfected with 1 μg of the linearized pCMV-rGsα by Effectene transfection reagent (Qiagen, Hilden, Germany) at subconfluency. Forty-eight hours after transfection, hygromycin was added to the medium at 200 μg/ml. Sensitive cells started dying 2 days after treatment. Seven days after treatment, resistant colonies were picked. These colonies were cultured without leukemia inhibitory factor (LIF) to allow differentiation into fibroblast-like cells before Western blot and assessment of cAMP production. To detect integration of the expression vector, PCR for the rat Gsα gene (sense primer, 5′-ggcaacagtaagaccgagga-3′; antisense primer, 5′-ccttggcatgctcatagaattc-3′) was performed (annealing, 60°C; extension, 72°C; denaturing, 94°C).

Generation of Chimeric Mice. Chimeras were generated by blastocyst injection as described in ref. 21. $Gnas^{+/patE2-}$, $Gnas^{matE2-/+}$, and $Gnas^{E2-/E2-}$ ES cells were injected into CD1-C57BL/6 F_1 hybrid blastocysts. To distinguish cells derived from host blastocysts and cells derived from ES cells, a β-galactosidase transgene was introduced into all wild-type hosts by mating C57BL/6 male mice carrying one copy of a β-galactosidase transgene (22) with wild-type CD1 females. The presence of the transgene was confirmed by staining for β-galactosidase activity. To produce chimeras with differing levels of ES cell contribution, the number of ES cells injected into the blastocele cavity was varied between 5 and 15. At least two independently established ES cell lines of each genotype yielded an identical phenotype. Resultant chimeric mice were killed at various ages from embryonic day (E) 10 through the neonatal period. To illustrate changes in chondrocyte differentiation, examples of bones from E17.5 are illustrated here. All of the observations in the results were verified in at least five different chimeric mice. The degree of chimerism was estimated by staining for β-galactosidase activity or by *in situ* hybridization for *Gsα* mRNA.

Chondrocyte Isolation, RNA Extraction, and Real-Time PCR. Chondrocytes were isolated from wild-type, $Gnas^{+/patE2-}$, or $Gnas^{matE2-/+}$ newborn mice as described in ref. 23. Briefly, limbs were dissected and placed in Hanks' balanced salt solution (HBSS) (Invitrogen). Soft tissue was removed, and epiphyses of the long bones were microdissected, followed by 0.25% trypsin-EDTA (Invitrogen) digestion for 30 min. Isolated cartilage was then digested with 195 units/ml collagenase type II (Worthington) in HBSS for 2 h at 37°C. Total RNA was extracted by using the RNeasy Mini RNA isolation kit (Qiagen). Reverse transcription of 1 μg of total RNA was performed by using the SuperScript First-Strand Synthesis System for RT-PCR (Invitrogen). Real-time PCR was carried out on a DNA Engine Opticon 2 system (MJ Research, Waltham, MA). The QuantiTect SYBR Green PCR kit (Qiagen) was used with cycling conditions as recommended by the manufacturer; annealing was performed at 60°C. Forward PCR primers for amplification of Gsα and XLαs transcripts were 5′-gcagaaggacaagcaggtct-3′ and 5′-ctcatcgacaagcaactgga-3′, respectively. Both reactions used the same reverse primer, 5′-ccctctccgttaaacccatt-3′. Primers for amplification of β-actin transcript were 5′-gatctggcaccacaccttct-3′ (forward) and 5′-ggggtgttgaaggtctcaaa-3′ (reverse). Normalized gene expression relative to β-actin was calculated with Q-GENE software (24). Amplification efficiencies by using plasmid templates were equal for all transcripts. Genotypes of mice were confirmed by PCR with tail DNA and the following primers for amplification of the neomycin-resistance gene inserted in *Gnas* exon 2 as part of the knockout strategy (16): 5′-aaggtgagatgacaggagatc-3′ (forward) and 5′-gatcggccattgaacaagatg-3′ (reverse).

Western Blot Analysis. Western blot analysis was performed on cell extracts from ES cells. Whole cell lysates (10 μg) were separated by 10% SDS/PAGE and transferred onto poly(vinylidene difluoride) filters. The filters were incubated with anti-HA tag antibody (1:500, Wako Biochemicals, Osaka), anti-actin (1:1,000, Santa Cruz Biotechnology), and anti-Gsα antibody (1:1,000, Santa Cruz Biotechnology). Antigen–antibody complexes were detected with horseradish peroxidase-conjugated secondary antibodies and visualized by using ECL Plus (Amersham Biosciences).

cAMP Assay. Accumulation of cAMP in hygromycin-resistant ES cells was measured in the presence of 2 mM isobutyl methyl xanthine (IBMX, Sigma). Control cells in 24-well plates were treated at room temperature for 1 h before termination of the reaction by adding 50 mM HCl. For PTH-stimulated cAMP accumulation, a 1-h period incubation with 10^{-8} M synthetic PTH analog, [Y34]hPTH(1–34)amide (synthesized at the MGH Biopolymer Core Facility, Boston), was performed at room temperature. The PTH-containing medium was then removed, and the stimulation was terminated by adding 50 mM HCl. The amount of cAMP in each well was determined by using RIA as described in ref. 25.

Southern Blot Analysis. Southern blot analysis was performed as described in ref. 26. To detect disrupted alleles of *Gnas* exon 2, 10 μg of genomic DNA was digested with *Xmn*I, Southern blotted, and probed with a *Not*I–*Sma*I fragment encoding the 5′ promoter region of the *Gnas* gene (16). The sizes of genomic DNA fragments expected from the normal and disrupted alleles are 11 and 9 kb, respectively (12).

Histological Analysis. Chimeric mice were killed at various ages, dissected, and fixed in 4% paraformaldehyde/PBS at 4°C for 4 h. For detection of β-galactosidase activity, tissues were stained with X-Gal (5-bromo-4-chloro-3-indolyl β-D-galactoside) as described in ref. 27. Subsequently, they were processed, embedded in paraffin, and cut. Sections were stained with hematoxylin/eosin (H&E) or nuclear fast red for morphological study.

To measure and compare the distances of hypertrophic chondrocytes from the articular surface, growth plates were obtained from five different chimeras for each genotype, stained for β-galactosidase activity plus H&E, and sectioned in the median plane. The distance of the earliest hypertrophic chondrocytes (detected based on morphology) from the articular surface was measured under the microscope. The earliest hypertrophic chondrocytes were defined as those located closest to the articular surface. The measurements were performed by three of the investigators blinded with regard to the genotypes. The significance of difference was assessed by using Student's *t* test.

***In Situ* Hybridization.** Tissues were fixed in 4% paraformaldehyde/PBS overnight at 4°C, processed, embedded in paraffin, and sectioned. *In situ* hybridization was performed as described in ref. 28 by using complementary ^{35}S-labeled riboprobes for rat *Gsα* (full-length cDNA), rat *XLαs* (nucleotides 380–1154, Gen-

DEVELOPMENTAL BIOLOGY

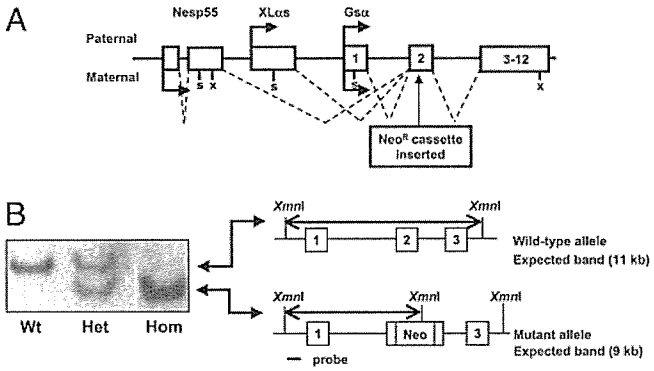

Fig. 1. Isolation of *Gnas*-mutant ES cells and generation of chimeras. (*A*) Schematic diagram of the *Gnas* locus. S, translation start site; X, termination codon. 1, 2, and 3–12 denote the number of the exons. Exons of the antisense and the 1A transcripts are not shown. (*B Left*) Southern blot analysis of isolated ES cells for the mutation in *Gnas* exon 2. Wt, wild-type; Het, heterozygous mutant; Hom, homozygous mutant. (*B Right*) The restriction map of the *Gnas* locus. *Xmn*I denotes the restriction site by *Xmn*I endonuclease.

Bank accession no. X84047), mouse *type X collagen*, mouse *Patched1* (*Ptc1*), mouse *Ihh*, mouse *osteopontin*, rat *PPR*, and mouse *PTHrP* (29).

Image Acquisition. An Axioskop 2 Plus (Zeiss) was used for microscopic observation (bright fields and dark fields at 100-fold magnification). Pictures were taken with an Axiocam HRc (Zeiss) camera, and images were acquired with AXIOVISION 3.0 software (Zeiss).

Results

Isolation of *Gnas*-Mutant ES Cells and Generation of Chimeras. A schematic representation of the *Gnas* locus is shown in Fig. 1*A*. $Gnas^{E2-/E2-}$ ES cells were generated *de novo* from inner cell masses of blastocysts derived by mating $Gnas^{+/E2-}$ mice with each other. Two of six isolated ES cell lines were $Gnas^{E2-/E2-}$. To obtain $Gnas^{+/patE2-}$ ES cells, $Gnas^{+/E2-}$ males were mated with wild-type females. Two of four isolated ES cell lines were $Gnas^{+/patE2-}$. To obtain $Gnas^{matE2-/+}$ ES cells, $Gnas^{+/E2-}$ females were mated with wild-type males. Two of five isolated ES cell lines were $Gnas^{matE2-/+}$. Genotypes were confirmed by Southern blot (Fig. 1*B*). To visually distinguish between cells derived from host blastocysts and cells derived from ES cells, one copy of a β-galactosidase transgene, engineered to be widely expressed in mouse tissues (22), was introduced into host blastocysts by appropriate mating. Generated ES cells were then injected into host blastocysts tagged with β-galactosidase. Thus, chimeric mice contain β-galactosidase-tagged wild-type cells (derived from blastocysts) and nontagged mutant cells (derived from ES cells).

Embryos containing both wild-type and $Gnas^{E2-/E2-}$ cells exhibited severe patterning defects resembling the overactivation of hedgehog signaling. If the chimerism was very high (>90%), the embryos were absorbed by E10, as $Gnas^{E2-/E2-}$ embryos were (data not shown). The embryos with chimerism between 10% and 90% exhibited severe patterning defects, including exencephaly, and did not survive beyond birth. Embryos containing wild-type and $Gnas^{E2-/+}$ cells at any ratio did survive beyond birth and grew into adulthood. Unlike $Gnas^{E2-/+}$ mice, these chimeric mice did not show significant growth defects, probably because of the predominant contribution of wild-type cells. For these reasons, we focused on the study of embryos. To illustrate hypertrophic differentiation of growth plate chondrocytes, we show representative data from E17.5, because the phenotypes of chondrocyte differentiation were similar at different ages, and embryos at E17.5 contain chondrocytes at various differentiation stages.

$Gnas^{E2-/E2-}$ Chondrocytes Undergo Ectopic Hypertrophy and Mimic $PPR^{-/-}$ Chondrocytes. The wild-type fetal growth plate consists of four major layers of chondrocytes with distinct morphology and gene expression profiles: from the end of bone, periarticular proliferating, columnar proliferating, prehypertrophic, and hypertrophic layers (29). The PTHrP signal directly prevents the switch from proliferation to hypertrophy of columnar proliferating chondrocytes (20). In the growth plate of chimeric mice containing wild-type and $PPR^{-/-}$ cells, mutant chondrocytes ectopically and prematurely adopted the hypertrophic phenotype (detected by their characteristic morphology and type X collagen expression), as they progress from the surrounding layer of wild-type periarticular proliferating chondrocytes to the surrounding layer of wild-type columnar proliferating chondrocytes (Fig. 2*A*). In the growth plates

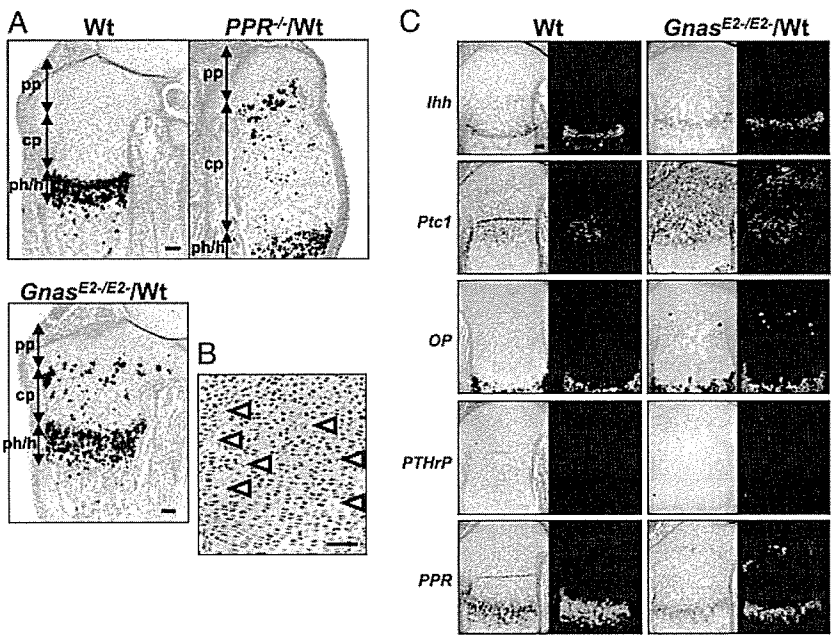

Fig. 2. $Gnas^{E2-/E2-}$ cells phenocopy $PPR^{-/-}$ cells in cartilage. (*A*) *In situ* hybridization for type X collagen mRNA of tibial sections from E17.5 wild-type, $PPR^{-/-}$/wild-type chimera, and $Gnas^{E2-/E2-}$/wild-type chimera embryos. pp, Periarticular proliferating chondrocytes; cp, columnar proliferating chondrocytes; ph/h, prehypertrophic and hypertrophic chondrocytes. (Scale bars, 100 μm.) (*B*) Staining for β-galactosidase activity plus H&E staining of sections from E17.5 $Gnas^{E2-/E2-}$/wild-type chimeric embryo. Wild-type cells were stained blue because of the presence of the β-galactosidase transgene. Arrowheads indicate ectopic hypertrophic chondrocytes. (Scale bar, 100 μm.) (*C*) *In situ* hybridization for Indian hedgehog (Ihh), Patched 1 (Ptc1), osteopontin (OP), PTHrP, and PPR mRNAs of tibial sections from E17.5 wild-type and $Gnas^{E2-/E2-}$/wild-type chimera embryos. (Scale bar, 100 μm.)

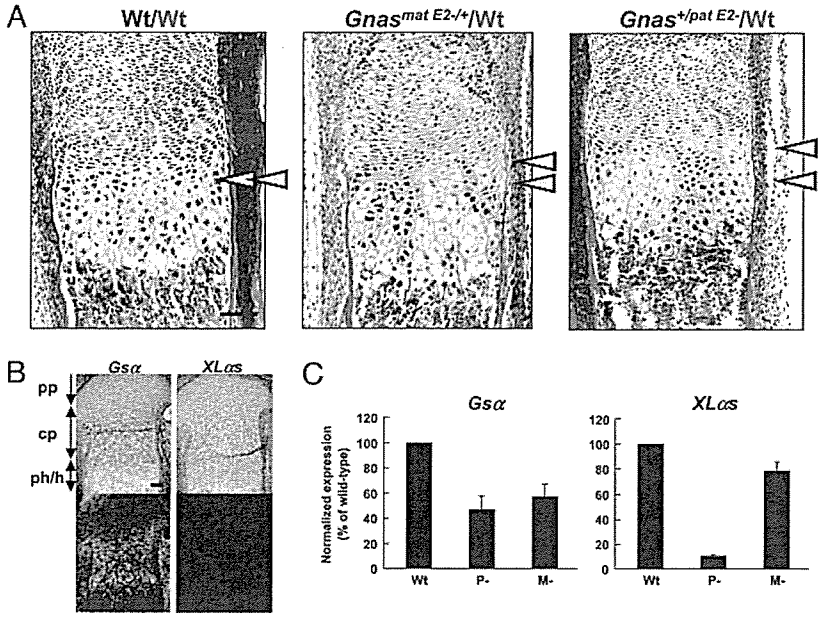

Fig. 3. Abnormal hypertrophy of $Gnas^{+/E2-}$ chondrocytes. (*A*) H&E staining of the radii from E17.5 wild-type/wild-type (*Left*), $Gnas^{matE2-/+}$/wild-type (*Center*), and $Gnas^{+/patE2-}$/wild-type (*Right*) chimeric embryos. Cells derived from host blastocysts were stained blue with 5-bromo-4-chloro-3-indolyl β-D-galactoside (X-Gal). The earliest hypertrophic chondrocytes (detected by their characteristic morphology) derived from host blastocysts and ES cells were marked with blue and white arrowheads, respectively. (Scale bar, 100 μm.) (*B*) *In situ* hybridization for Gsα mRNA and XLαs mRNA of tibial sections from E17.5 wild-type embryos. Upper panels, bright fields; lower panels, dark fields. pp, Periarticular proliferating chondrocytes; cp, columnar proliferating chondrocytes; ph/h, prehypertrophic and hypertrophic chondrocytes. (Scale bar, 100 μm.) (*C*) Real-time RT-PCR analysis of Gsα and XLαs mRNAs expressed in limb chondrocytes isolated from wild-type (Wt), $Gnas^{+/patE2-}$ (P−), or $Gnas^{matE2-/+}$ (M−) newborn mice.

of chimeric mice containing wild-type cells and $Gnas^{E2-/E2-}$ cells, mutant chondrocytes similarly adopted the hypertrophic phenotype at an ectopic location (Fig. 2*A*). Based on the observations of stained and nonstained cells for β-galactosidase activity, all ectopically hypertrophied cells were mutant (Fig. 2*B*, arrowheads), whereas all wild-type cells maintained their expected morphology. $Gnas^{E2-/E2-}$ ectopic hypertrophic chondrocytes expressed other markers of hypertrophy such as Indian hedgehog (Ihh) and osteopontin, and induced Ihh's transcriptional target Patched 1 (Ptc1) in surrounding wild-type cells, as did $PPR^{-/-}$ ectopic hypertrophic chondrocytes. PTHrP mRNA expression was up-regulated in the periarticular layer (Fig. 2*C*). Thus, $Gnas^{E2-/E2-}$ cells phenocopied $PPR^{-/-}$ cells with respect to premature hypertrophic differentiation. Unlike $PPR^{-/-}$ ectopic hypertrophic chondrocytes, however, $Gnas^{E2-/E2-}$ ectopic hypertrophic chondrocytes expressed PPR mRNA (Fig. 2*C*).

$Gnas^{+/E2-}$ Chondrocytes also Undergo Premature Hypertrophy, but to a Lesser Extent Than $Gnas^{E2-/E2-}$ Chondrocytes. AHO is associated with heterozygous inactivating mutations in any one of the *GNAS* exons encoding Gsα and a large portion of XLαs (except for exon 3, which can be alternatively spliced out and still produce functional Gsα) (6). Although abnormal chondrocyte development may contribute to the AHO phenotype, there has been no clear *in vivo* evidence that $Gnas^{+/E2-}$ chondrocytes are functionally defective. The chimeric strategy provided us with an opportunity to identify even subtle differences between wild-type and $Gnas^{+/E2-}$ chondrocytes by comparing them side by side *in vivo*. Wild-type cells derived from ES cells differentiated in a way that was indistinguishable from that of wild-type cells derived from host blastocysts (Fig. 3*A*). In the growth plates of chimeric mice containing wild-type and $Gnas^{+/E2-}$ cells, both $Gnas^{+/patE2-}$ chondrocytes and, to a lesser extent, $Gnas^{matE2-/+}$ chondrocytes adopted a hypertrophic morphology at a location closer to the ends of bone than wild-type cells (Fig. 3*A*). The distances of hypertrophic chondrocytes from the articular surface in the ulnae and radii were 78 ± 3% for $Gnas^{+/patE2-}$ cells and 91 ± 2% for $Gnas^{matE2-/+}$ cells compared with that of wild-type cells derived from host blastocysts within the same growth plates ($n = 5, P < 0.05$ by Student's *t* test); the difference in the distances from the articular surface of $Gnas^{matE2-/+}$ and $Gnas^{+/patE2-}$ hypertrophic chondrocytes was also significant ($n = 5, P < 0.05$ by Student's *t* test). These findings suggested that Gs signaling in the growth plate is subject to haploinsufficiency.

Expression of Gsα and XLαs in the Growth Plate Cartilage. Based on the data presented above, it appears that Gsα plays a major physiologic role in regulation of hypertrophic differentiation of growth plate chondrocytes. However, other gene products from the *Gnas* locus may be responsible for the phenotypes in $Gnas^{E2-/E2-}$ chondrocytes, because exon 2 is common to several different transcripts. Particularly, XLαs, encoded by transcripts that use a unique first exon and exons 2–12 of Gsα, is identical to the latter over a long stretch of C-terminal amino acids (6). Moreover, XLαs has been shown to have "Gs-like" signaling properties *in vitro* (17, 18). To determine the spatial distribution and relative expression of XLαs and Gsα mRNA in the growth plate, *in situ* hybridization and real-time RT-PCR analysis were performed. In wild-type mice, Gsα mRNA was expressed in the entire growth plate, with its highest expression in prehypertrophic chondrocytes; in contrast, XLαs mRNA appeared to be expressed at lower levels than Gsα mRNA, and its highest expression was in early hypertrophic chondrocytes (Fig. 3*B*). Mean normalized expression levels of Gsα and XLαs mRNA relative to β-actin mRNA in wild-type chondrocytes were 8.76 ± 1.37% ($n = 4$) and 0.37 ± 0.02% ($n = 4$), respectively, thus indicating a >20-fold difference between the expression levels of XLαs and Gsα in this tissue. Previously, monoallelic expression of Gsα has been shown in several different tissues. Based on the phenotype observed in chimeric growth plates (Fig. 3*A*), Gsα does not appear to be imprinted in growth plate chondrocytes. To confirm biallelic expression of Gsα *in vivo*, limb chondrocytes were isolated from wild-type, $Gnas^{+/patE2-}$, or $Gnas^{matE2-/+}$ newborn mice for real-time RT-PCR analysis. Gsα mRNA expression was reduced to approximately half that of the wild type in both $Gnas^{+/patE2-}$ (46 ± 11%, $n = 5$) and $Gnas^{matE2-/+}$ (57 ± 10%, $n = 5$) chondrocytes (Fig. 3*C*), indicating biallelic expression of Gsα in these cells. In contrast, XLαs expression in $Gnas^{matE2-/+}$ chondrocytes was comparable to that of the wild type (78 ± 10%, $n = 5$), and XLαs expression in $Gnas^{+/patE2-}$ chondrocytes was reduced dramatically (10 ± 1%, $n = 5$) (Fig. 3*C*), consistent with the paternal expression of XLαs transcripts documented previously in a number of different tissues.

Introduction of Gsα into $Gnas^{E2-/E2-}$ Chondrocytes Rescues Ectopic Hypertrophy. To determine whether Gsα protein alone can reverse the phenotype seen in $Gnas^{E2-/E2-}$ chondrocytes, $Gnas^{E2-/E2-}$ cells

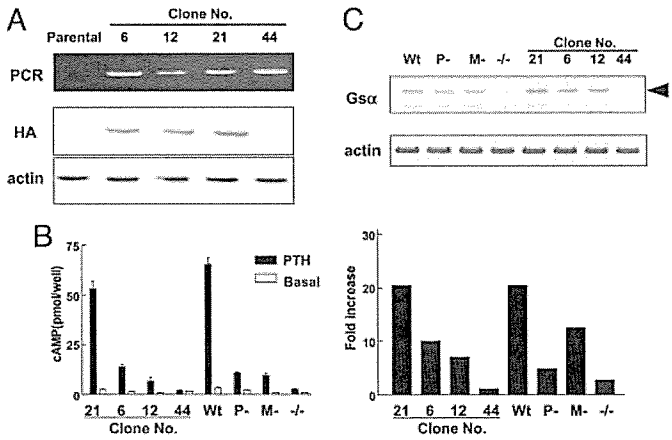

Fig. 4. Rescue of Gs signaling in $Gnas^{E2-/E2-}$ cells by rat Gsα. (*A*) Integration of pCMV-rGsα transgene was detected by PCR of genomic DNA for rat Gsα (*Top*), and expression of the transgene was detected by Western blot analysis for HA tag (*Middle*), in ES cell lines differentiated into fibroblast-like cells. (*B*) cAMP response of various differentiated ES cell lines to PTH. Absolute basal and stimulated cAMP levels are shown on the left, and fold-stimulation is shown on the right. Clones 21, 6, 12, and 44 were $Gnas^{E2-/E2-}$ ES cell lines stably transfected with pCMV-rGsα. (*C*) Comparison of expression levels of Gsα and endogenous mouse Gsα proteins detected by Western blot for Gsα. Arrowhead indicates the longer variant.

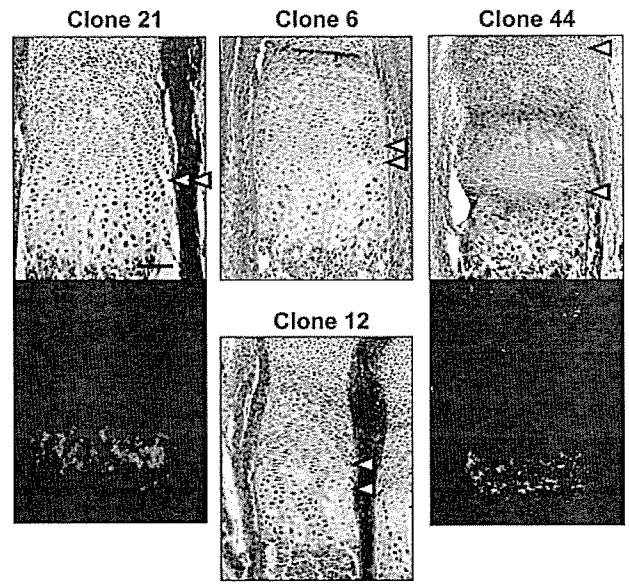

Fig. 5. Rescue of $Gnas^{E2-/E2-}$ chondrocytes by rat Gsα. Shown is staining for β-galactosidase activity plus H&E staining of a section of the radii from an E17.5 $Gnas^{E2-/E2-}$; pCMV-rGsα/wild-type chimeric embryo. Cells derived from host blastocysts were stained blue with 5-bromo-4-chloro-3-indolyl β-D-galactoside (X-Gal). The earliest hypertrophic chondrocytes (detected by their characteristic morphology) derived from host blastocysts and ES cells were marked with blue and white arrowheads, respectively. The lower portions of the panels for clones 21 and 44 show *in situ* hybridization for type X collagen mRNA in serial sections. (Scale bar, 100 μm.)

were transfected with rat Gsα cDNA placed under the control of the CMV promoter. Stable transfectants were selected in the presence of hygromycin, and the integration of the transgene was confirmed by PCR of genomic DNA isolated from these transfectants (Fig. 4*A*). We refer to these ES cell lines as $Gnas^{E2-/E2-}$; pCMV-rGsα. After expansion of 54 resistant colonies and differentiation into fibroblastic cells, we measured cAMP production in response to PTH. Expression of rat Gsα protein was assessed by Western blot for the HA tag (Fig. 4*A*).

Among 54 ES cell clones isolated, we chose four representative $Gnas^{E2-/E2-}$; pCMV-rGsα clones based on their responses to PTH treatment: clone 21 showed robust PTH-induced cAMP accumulation similar in extent to that in wild-type ES cells; clones 6 and 12 showed PTH-induced cAMP responses that were less pronounced than in wild-type cells but similar to that in $Gnas^{+/E2-}$ ES cells; and clone 44 failed to respond to PTH, just as did $Gnas^{E2-/E2-}$ cells (Fig. 4*B*). Gsα protein levels roughly corresponded to their respective responses to PTH (Fig. 4*C*). By injecting these transfected ES cells into wild-type blastocysts, we generated chimeric mice to assess the functional consequences. In contrast to $Gnas^{E2-/E2-}$ chondrocytes, $Gnas^{E2-/E2-}$; CMV-rGsα (clone 21) chondrocytes did not undergo ectopic hypertrophy, whereas clones 6 and 12 partially did. The distances of hypertrophic chondrocytes from the articular surface in the ulnae and radii were 82 ± 3% for clone 6 and 88 ± 2% for clone 12, compared with that of wild-type cells derived from host blastocysts within the same growth plates ($n = 5$, $P < 0.05$ by Student's *t* test). Clone 44 chondrocytes, on the other hand, behaved similarly to the $Gnas^{E2-/E2-}$ chondrocytes (Fig. 5). These data further suggest that Gsα, rather than the other *Gnas* gene products, is the major signaling molecule at the *Gnas* locus controlling chondrocyte hypertrophy.

Discussion

In this study, we investigated the *in vivo* roles of Gsα on differentiation of growth plate cartilage. Although haploinsufficiency of Gsα signaling in growth plate chondrocytes was suspected as being important for the development of AHO features, there has been no clear *in vivo* evidence for this hypothesis. In addition, although the allelic pattern of expression of Gsα in several other tissues have been studied, the pattern of expression in chondrocytes had not previously been investigated. Taking advantage of the chimeric technique, we discerned a difference between wild-type and $Gnas^{+/E2-}$ chondrocytes in intact animals and showed that $Gnas^{+/E2-}$ chondrocytes differentiate prematurely. Using chondrocytes from either $Gnas^{+/patE2-}$ or $Gnas^{matE2-/+}$ mice, we also demonstrated that Gsα expression in these cells is biallelic, i.e., transcripts are derived from both parental alleles. Previously, a growth plate abnormality could not be shown in $Gnas^{+/E2-}$ mice *in vivo* (16). There are two possible explanations for the apparent lack of a growth plate phenotype in those animals. First, the abnormality may be too subtle to be detected by conventional techniques. The chimeric technique successfully enhances the sensitivity of detection by comparing wild-type and mutant cells side by side *in vivo*. Second, other interacting signaling pathways may compensate for the abnormality in Gsα signaling. For example, PTHrP-PPR-Gsα signaling interacts with hedgehog signaling to form a negative feedback loop (29). The acceleration of hypertrophic differentiation due to impaired Gsα signaling results in a concomitant increase in Hh signaling and PTHrP expression that may partially compensate for the loss of Gsα signaling and may thereby obscure the Gsα haploinsufficiency. With the chimeric technique, these compensating mechanisms are not a major influence, as long as the abnormality is cell-autonomous, because cells of different genotypes are placed in the same milieu.

The difference between $Gnas^{+/patE2-}$ and $Gnas^{matE2-/+}$ chondrocytes is modest but statistically significant. The reason for this difference may be other imprinted transcripts derived from the *Gnas* locus. For example, Nesp55 is derived only from the maternal allele, whereas XLαs is derived only from the paternal allele. Although the *Nesp55* gene uses exons 2–12 of *Gsα*, these exons are in the 3′ UTR, and the disruption of exon 2 does not affect the expression of Nesp55 (T. Xie and L.S.W., unpublished observations). Therefore, it is unlikely that the disruption of NESP55

contributes to the difference in phenotypes between $Gnas^{+/patE2-}$ and $Gnas^{matE2-/+}$ chondrocytes. On the other hand, XLαs shares exons 2–12 with Gsα, which are translated, and XLαs couples to several G protein-coupled receptors and stimulates adenylyl cyclases *in vitro* with an efficiency similar to that of Gsα (18). Moreover, XLαs and Gsα mRNAs show only a slightly different pattern of expression in the growth plate, although the level of expression of XLαs is much lower. Thus, the difference between $Gnas^{+/patE2-}$ and $Gnas^{matE2-/+}$ chondrocytes may reflect the modest additional effect of the paternally derived XLαs on regulation of hypertrophy, suggesting that there may be redundancy between Gsα and XLαs in the growth plate.

The PPR is known to couple with Gq/11 *in vitro* as well as Gs (1, 2). Mice carrying a mutant PPR selectively deficient in signaling through Gq/11 show a modest delay in hypertrophic differentiation of growth plate chondrocytes (5), whereas the $Gnas^{+/E2-}$ chondrocytes are expected to normally activate Gq/11 in response to PTHrP. Acceleration of hypertrophy as a result of disproportionate signaling through Gq/11 may thus contribute to the chimeric phenotype. Nevertheless, the close resemblance between mutant chondrocytes in the $PRR^{-/-}$ chimeras and $Gnas^{E2-/E2-}$ chimeras suggests that Gsα is the dominant signaling system downstream of the PPR in chondrocytes. It is noteworthy that the columns of wild-type proliferating chondrocytes in the growth plates of the $Gnas^{E2-/E2-}$/wild-type chimeras are not elongated. This observation contrasts with the elongation of wild-type columnar proliferating layer of the growth plate seen in $PPR^{-/-}$/wild-type chimeras. This elongation seen in $PPR^{-/-}$/wild-type chimeras is probably due to the effect of an increased level of PTHrP expression on wild-type cells. The difference between the two chimeric growth plates presumably derives from the difference between the two kinds of mutations studied. $Gnas^{E2-/E2-}$ chondrocytes express normal PPRs, whereas $PRR^{-/-}$ chondrocytes lack PPRs. Thus, the PPR of the $Gnas^{E2-/E2-}$ chondrocytes can be expected to signal through Gq. This Gq signal from $Gnas^{E2-/E2-}$ chondrocytes may lead to suppression of elongation of adjacent wild-type columns. Alternatively, the PPR may sequester PTHrP and constrain PTHrP from diffusing. $PRR^{-/-}$ chondrocytes cannot bind PTHrP through PPR, whereas $Gnas^{E2-/E2-}$ chondrocytes still can. Through these mechanisms or perhaps others, the columns of wild-type proliferating chondrocytes in the growth plates of the $Gnas^{E2-/E2-}$/wild-type chimeras did not elongate.

Mice carrying a null mutation in *Gnas* exon1 have been generated (¶ and M. Chen and L.S.W., unpublished results). Exon 1, unlike *Gnas* exons 2–12, is specific to Gsα. The preliminary analysis of the mutant mice has shown that homozygous mice display embryonic lethality and in that way resemble $Gnas^{E2-/E2-}$ mice. However, heterozygous mice with exon 1 disruption on the paternal allele have a distinct phenotype from $Gnas^{+/patE2-}$. These data are in contrast to the findings in humans with AHO, for whom no correlation between severity of phenotypes and the location of affected exons, including exon 1, has been noticed thus far. These differences may reflect species-specific differences in the physiological and developmental roles of alternative *GNAS/Gnas* gene products. Generation of chimeric mice containing $Gnas^{+/E1-}$ and comparison of these mice with $Gnas^{+/E2-}$ chimeric mice will provide further insights into specific functions of Gsα and the other transcripts.

In summary, our results indicate that Gsα plays an essential role in differentiation of growth plate chondrocytes *in vivo* and that it is the primary mediator of the actions of PPR in this tissue. In addition, we show that, unlike in several other tissues where Gsα expression occurs predominantly from the maternal allele, expression of Gsα mRNA in chondrocytes occurs from both parental alleles. Furthermore, we provide strong evidence suggesting that haploinsufficiency of Gsα signaling in growth plate chondrocytes contributes to the skeletal phenotypes of AHO.

¶Schwindinger, W. F., Lawler, A. M., Gearhart, J. D. & Levine, M. A., 80th Annual Meeting of the Endocrine Society, New Orleans, June 24–27, 1998, p. 480 (abstr.).

We thank Dr. Ernestina Schipani for technical assistance in chondrocyte isolation. This work was supported by National Institutes of Health Grants AR47078, DK56246, and DK46718.

1. Jüppner, H., Abou-Samra, A. B., Freeman, M., Kong, X. F., Schipani, E., Richards, J., Kolakowski, L. F., Jr., Hock, J., Potts, J. T., Jr., Kronenberg, H. M., *et al.* (1991) *Science* **254,** 1024–1026.
2. Abou-Samra, A. B., Jüppner, H., Force, T., Freeman, M. W., Kong, X. F., Schipani, E., Urena, P., Richards, J., Bonventre, J. V., Potts, J. T., Jr., *et al.* (1992) *Proc. Natl. Acad. Sci. USA* **89,** 2732–2736.
3. Karaplis, A. C., Luz, A., Glowacki, J., Bronson, R. T., Tybulewicz, V. L., Kronenberg, H. M. & Mulligan, R. C. (1994) *Genes Dev.* **8,** 277–289.
4. Lanske, B., Karaplis, A. C., Lee, K., Luz, A., Vortkamp, A., Pirro, A., Karperien, M., Defize, L. H., Ho, C., Mulligan, R. C., *et al.* (1996) *Science* **273,** 663–666.
5. Guo, J., Chung, U. I., Kondo, H., Bringhurst, F. R. & Kronenberg, H. M. (2002) *Dev. Cell* **3,** 183–194.
6. Weinstein, L. S., Yu, S., Warner, D. R. & Liu, J. (2001) *Endocr. Rev.* **22,** 675–705.
7. Levine, M. A. (1999) *Arch. Med. Res.* **30,** 522–531.
8. Bastepe, M. & Jüppner, H. (2000) *Endocrinol. Metab. Clin. North Am.* **29,** 569–589.
9. Mantovani, G., Ballare, E., Giammona, E., Beck-Peccoz, P. & Spada, A. (2002) *J. Clin. Endocrinol. Metab.* **87,** 4736–4740.
10. Germain-Lee, E. L., Ding, C. L., Deng, Z., Crane, J. L., Saji, M., Ringel, M. D. & Levine, M. A. (2002) *Biochem. Biophys. Res. Commun.* **296,** 67–72.
11. Liu, J., Erlichman, B. & Weinstein, L. S. (2003) *J. Clin. Endocrinol. Metab.* **86,** 4336–4341.
12. Hayward, B. E., Barlier, A., Korbonits, M., Grossman, A. B., Jacquet, P., Enjalbert, A. & Bonthron, D. T. (2001) *J. Clin. Invest.* **107,** R31–R36.
13. Zheng, H., Radeva, G., McCann, J. A., Hendy, G. N. & Goodyer, C. G. (2001) *J. Clin. Endocrinol. Metab.* **86,** 4627–4629.
14. Linglart, A., Carel, J. C., Garabedian, M., Le, T., Mallet, E. & Kottler, M. L. (2002) *J. Clin. Endocrinol. Metab.* **87,** 189–197.
15. Levine, M. A. (2002) in *Principles of Bone Biology*, eds. Bilezikian, J. P., Raisz, L. G. & Rodan, G. A. (Academic, San Diego), Vol. 2, pp. 1137–1163.
16. Yu, S., Yu, D., Lee, E., Eckhaus, M., Lee, R., Corria, Z., Accili, D., Westphal, H. & Weinstein, L. S. (1998) *Proc. Natl. Acad. Sci. USA* **95,** 8715–8720.
17. Klemke, M., Pasolli, H. A., Kehlenbach, R. H., Offermanns, S., Schultz, G. & Huttner, W. B. (2000) *J. Biol. Chem.* **275,** 33633–33640.
18. Bastepe, M., Gunes, Y., Perez-Villamil, B., Hunzelman, J., Weinstein, L. S. & Jüppner, H. (2002) *Mol. Endocrinol.* **16,** 1912–1919.
19. Robertson, E. J. (1987) in *Teratocarcinomas and Embryonic Stem Cells*, ed. Robertson, E. J. (IRL, Oxford), pp. 71–112.
20. Chung, U. I., Lanske, B., Lee, K., Li, E. & Kronenberg, H. (1998) *Proc. Natl. Acad. Sci. USA* **95,** 13030–13035.
21. Bradley, A. (1987) in *Teratocarcinomas and Embryonic Stem Cells*, ed. Robertson, E. J. (IRL, Oxford), pp. 113–151.
22. Zambrowicz, B. P., Imamoto, A., Fiering, S., Herzenberg, L. A., Kerr, W. G. & Soriano, P. (1997) *Proc. Natl. Acad. Sci. USA* **94,** 3789–3794.
23. Pfander, D., Kobayashi, T., Knight, M. C., Zelzer, E., Chan, D. A., Olsen, B. R., Giaccia, A. J., Johnson, R. S., Haase, V. H. & Schipani, E. (2004) *Development (Cambridge, U.K.)* **131,** 2497–2508.
24. Muller, P. Y., Janovjak, H., Miserez, A. R. & Dobbie, Z. (2002) *BioTechniques* **32,** 1372–1374, 1376, 1378–1379.
25. Schipani, E., Kruse, K. & Jüppner, H. (1995) *Science* **268,** 98–100.
26. Yu, S., Gavrilova, O., Chen, H., Lee, R., Liu, J., Pacak, K., Parlow, A. F., Quon, M. J., Reitman, M. L. & Weinstein, L. S. (2000) *J. Clin. Invest.* **105,** 615–623.
27. Rossert, J., Eberspaecher, H. & de Crombrugghe, B. (1995) *J. Cell Biol.* **129,** 1421–1432.
28. Lee, K., Deeds, J. D. & Segre, G. V. (1995) *Endocrinology* **136,** 453–463.
29. Chung, U. I., Schipani, E., McMahon, A. P. & Kronenberg, H. M. (2001) *J. Clin. Invest.* **107,** 295–304.

Available online at www.sciencedirect.com
SCIENCE DIRECT®
Experimental Cell Research 295 (2004) 194–203
Experimental Cell Research
www.elsevier.com/locate/yexcr

Characterization of multipotent adult stem cells from the skin: transforming growth factor-β (TGF-β) facilitates cell growth

Yoko Kawase,[a,b] Yasuo Yanagi,[a] Tsuyoshi Takato,[b] Manabu Fujimoto,[a] and Hitoshi Okochi[a,*]

[a] *Department of Regenerative Medicine, Research Institute, International Medical Center of Japan, Tokyo 162-8655, Japan*
[b] *Department of Oral and Maxillofacial Surgery, Graduate School of Medicine, University of Tokyo, Tokyo 113-8655, Japan*

Received 3 October 2003, revised version received 17 December 2003

Abstract

Recently, adult stem cells have been isolated from the skin and designated as skin-derived precursors (SKPs). These SKPs, cultured in vitro, can give rise to neurons, glia, smooth muscle cells, and adipocytes. In the current study, we confirmed the clonal expansion of SKPs using a sphere-forming culture system in a medium containing methylcellulose. Among the growth factors, only transforming growth factor-β (TGF-β) was revealed to uniquely facilitate the sphere formation and proliferation of the SKPs in combination with EGF and bFGF. In addition, TGF-β did not alter phenotypical characteristics of the SKPs under sphere-forming conditions. The effect of TGF-β on sphere formation was not observed in neural stem cells, which expressed a different set of cell surface markers from SKPs, suggesting that SKPs have distinct features. Although the number of SKPs decreased with age, TGF-β increased the sphere colony formation and proliferation in all ages. These results suggest that SKPs maintained in the presence of TGF-β during culture are of potential use in cell-replacement therapies employing adult tissue sources.

Keywords: Adult stem cell; Aging; Dermis; Growth factor; Regenerative medicine; Skin-derived precursors

Introduction

Adult stem cells are an attractive source for cell-based therapies, in which autologous cells can be used to circumvent immunological problems. Adult stem cells can be isolated from various tissues. Recent studies have revealed that adult stem cells have a broader potential or plasticity than was previously considered. For example, neural stem cells have the ability to differentiate into cells belonging to all three germ layers, when transplanted in early embryos [1]. Similarly, cells isolated from bone marrow have been observed to give rise to neural cells [2–4], skeletal muscle cells [5], and hepatocytes [6]. Collectively, these findings suggest that various adult tissues can be used in autologous cell-replacement therapies.

From the point of view of practical therapeutic approach, the skin has many advantages as a potential stem cell source, including easy accessibility and high self-renewal ability. Several studies have demonstrated that epidermal stem cells are multipotent and in the bulge region of the hair follicle in vivo [7–10]. Mesenchymal stem cells isolated from adipose tissues can also differentiate in vitro into adipogenic, chondrogenic, myogenic, and osteogenic cells [11,12]. Recently, Toma et al. [13] have demonstrated that the stem cells can be also isolated from the dermis and expanded in vitro. These dermal cells proliferate to form "spheres" in suspension in vitro in the presence of epidermal growth factor (EGF) and basic fibroblast growth factor (bFGF). These cells, designated as skin-derived precursors (SKPs), can differentiate in culture into neurons, glia, smooth muscle cells, and adipocytes. Although the origin and nature of SKPs in vivo remain unknown, these observations raise the possibility that SKPs can be utilized as an autologous source of stem cells for transplantation.

In the current study, SKPs were further characterized especially in terms of their response to various growth

* Corresponding author. Department of Regenerative Medicine, Research Institute, International Medical Center of Japan, 1-21-1 Toyama, Shinjuku, Tokyo 162-8655, Japan. Fax: +81-3-3202-7192.
E-mail address: hokochi@ri.imcj.go.jp (H. Okochi).

0014-4827/$ - see front matter © 2004 Elsevier Inc. All rights reserved.
doi:10.1016/j.yexcr.2003.12.027

factors, by using a clonogenic sphere-forming assay. While either EGF or bFGF was essential for the growth of SKPs, the addition of transforming growth factor-β (TGF-β) specifically and markedly increased the formation and proliferation of SKPs, suggesting that TGF-β plays an important role in their growth.

Materials and methods

Animals

Wild-type (WT) mice (C57BL/6 background) and green fluorescent protein (GFP)–transgenic mice on a C57BL/6 background [14] purchased from Charles River laboratories, Inc. (Wilmington, MA) were used at 8–12 weeks of age except when indicated. All procedures were approved by the Animal Care and Use Committee of the International Medical Center of Japan.

Reagents

Primary monoclonal antibodies were: anti-nestin (Rat 401 clone; BD PharMingen, San Jose, CA), anti-fibronectin (10 clone; BD Bioscience, San Jose, CA), anti-neurofilament H (NF-H) (3G3 clone; Chemicon, Temecula, CA), anti-rat CD49f (GoH3 clone; BD PharMingen), biotin-conjugated anti-CD34 (RAM34 clone; BD PharMingen), fluorescein isothiocyanate (FITC)-conjugated anti-E-cadherin (36 clone; BD Bioscience), R-phycoerythein (R-PE)-conjugated anti-Thy1.2 (53–2.1 clone; BD PharMingen), FITC-conjugated anti-α-smooth muscle actin (αSMA) (1A4 clone; Sigma Aldrich, St. Louis, MO), FITC-conjugated anti-CD29 (Ha2/5 clone; BD PharMingen), and R-PE-conjugated anti-CD71 (C2 clone; BD PharMingen). Primary polyclonal antibodies were: anti-neuronal class III β-tubulin (Babco, Richmond, CA), anti-glial fibrillary acidic protein (GFAP) (Dako, Glostrup, Denmark), anti-neurofilament M (NFM) (Chemicon), and anti-microtubule-associated protein 2 (MAP2) (Biogenesis, Poole, England, UK). Secondary antibodies were: Alexa 594-conjugated donkey anti-mouse IgG (Molecular Probes, Eugene, OR), Alexa 594-conjugated donkey anti-rabbit IgG. (Molecular Probes), and R-PE-conjugated rabbit anti-rat IgG (Southern Biotechnology Associates, Inc., Birmingham, AL). For neutralization of TGF-β bioactivity, anti-TGF-β monoclonal antibody (9016.2 clone; Genzyme-Teche, Cambridge, MA) was used at 1 μg/ml.

Sources of growth factors and their final concentration were as follows: bFGF (10 ng/ml or 20 ng/ml), Transforming growth factor-α (TGF-α) (50 ng/ml), ciliary neurotrophic factor (CNTF) (50 ng/ml), brain-derived neurotrophic factor (BDNF) (50 ng/ml), neurotrophin-3 (NT-3) (50 ng/ml), TGF-β (0.001–10 ng/ml) (all from Peprotech EC LTD, London, UK), EGF (10 ng/ml; R&D System, Minneapolis, MN) nerve growth factor β (NGF-β) (5 ng/ml; Biosource, Camarillo, CA), bone morphogenetic protein 4 (BMP-4) (10 ng/ml; R&D System), and activin A (2 ng/ml; generously provided by Dr. M. Asashima, University of Tokyo).

Sphere formation from the skin

The preparation of SKPs was performed as described elsewhere [13] with minor modifications. Briefly, to obtain single cell suspensions, the skin from ears of mice were dissected, cut into 2–3 mm^3 pieces, washed three times in Hanks balanced buffered saline (HBSS; GIBCO BRL, Rockville, MD), and then digested with 0.1% trypsin for 60 min at 37°C. Tissue pieces were then mechanically dissociated in Dulbecco's modified eagle medium (DMEM)/F12 (GIBCO BRL) and washed once with trypsin neutralizing solution (TNS; Cell Applications, San Diego, CA). The cell suspension was poured through a 40-μm cell strainer (Becton Dickinson Labware, Franklin Lakes, NJ). Dissociated cells were chilled on ice for 20–30 min, centrifuged at 1000 rpm for 10 min, and resuspended in DMEM/F12 containing B27 supplement (GIBCO, BRL). These cells were plated at a cell density of 10 cells/μl on uncoated 24-well dishes and cultured in DMEM/F12 containing 1.5% methylcellulose (Wako, Osaka, Japan) and B27 supplement. bFGF and EGF at a final concentration of 10 and 20 ng/ml, respectively, were added to the medium three times a week for 14 days. TGF-β and other growth factors were added 3 days after the initial plating or the cell passage where indicated. To passage the spheres, sphere colonies obtained after 14 days in culture were collected, dissociated into single cells by trypsinization, plated in 24-well dishes at a cell density of 10 cells/μl and cultured for further 7–10 days under the same conditions. Cells were passaged every 7 days thereafter. To measure the diameters of the sphere colonies, the cultures were observed with an inverted microscope (IX70, Olympus, Tokyo, Japan), and the images were analyzed by NIH image program developed at the U.S. National Institutes of Health and available on the Internet at http://rsb.info.nih.gov/nihimage/.

Neurosphere formation from embryonic striatal germinal zone

Embryos were removed from each uterine horn from each dam at embryonic day 14. The striatal primordium was dissected from each embryo in HBSS as described previously [15]. The tissue from each embryo was transferred to a serum-free medium, DMEM/F12 and mechanically triturated into single cell. These cells were plated at a cell density of 10 cells/μl on uncoated 24-well dishes and cultured in DMEM/F12 containing 0.8% methylcellulose and B27 supplement. bFGF and EGF at a final concentration of 20 ng/ml were added to the medium three times a week. After 6–8 days, the cells formed neurospheres.